Study, Design and Modeling of Thermal Effects in III-V based HEMT Devices for Opto-Telecommunication Applications

Syed Hassan Murtaza
Reg. No:
12-FET/MSEE/F06

Supervisor

Prof. Dr. Ahmed Shuja Syed
Adjunct Professor & Former Dean
FET, IIUI, Islamabad

Advance Electronics Laboratory
Department of Electronic Engineering
Faculty of Engineering and Technology, (FET)

International Islamic University, (IIU), Islamabad

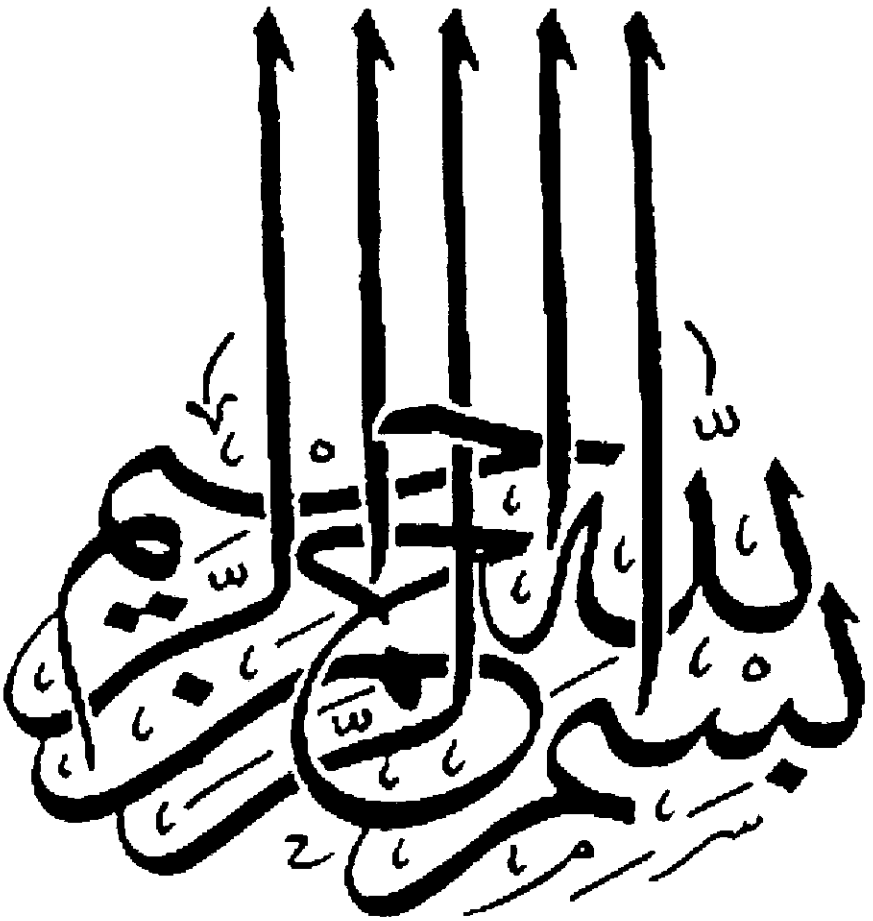

In The Name of **Allah**;

The Most Gracious, Most Merciful

CERTIFICATE OF APPROVAL

Title of Thesis : Study, Design and modeling of thermal effects in III-V HEMT devices For opto-telecommunication Application

Name of Student: Syed Hassan Murtaza Bokhari

Registration No :. 12-FET-MSEE-F06

Accepted by the Faculty of Electronic Engineering, INTERNATIONAL ISLAMIC UNIVERSITY, ISLAMABAD in partial fulfillment of the requirements for the degree of Master of Science with specialization in Communication and Signal Processing.

Viva Voce Committee

Dean
Dr. Ghulam Yasin Chohan
FET

Chairman
Dr. Muhammad Zubair
DEE, FET

External Examiner
Dr. Sajjad Asghar
Scientist, Nescom

Internal Examiner
Dr. Ihsan ul Haq
DEE, FET

Supervisor
Prof. Dr. Ahmed. Syed
Adjunct Faculty DEE, FET iiui

Dedicated to my Respectable Parents

ACKNOWLEDGEMENTS

I am grateful to Allah. who permits me to live and accomplish tasks including the research work being presented in this thesis.

Dr. Prof. Ahmed Shuja Syed, My MS supervisor is the person who was always there to help me during my research work. I would have been no where without him. I am very proud to work under his supervision.

I am also grateful to the senior faculty members of FET, IIUI for their continuous support without which completion of my MS degree would not have been possible.

May Allah bless the above wonderful people!

Syed Hassan Murtaza

Table of Contents

List of Figures

List of Tables

ABSTRACT

The ion implanted AlGaN/GaN High Electron Mobility Transistors (HEMT) test structures were studied thoroughly to look into the possibilities of enhancing the HEMT efficiency for high-power and high-frequency electronic applications. A dedicated experimental design was created in order to study the influence of the physical parameters in response to the high energy (by virtue of in-situ beam heating due to highly energetic implantation) ion implantation to the active device regions in nitride HEMT structures. A very calculated disorder or damage created in the HEMT structure was then studied carefully with Electrical characterization techniques such as Hall, I-V and G-V measurements. The evolution of the electrical characteristics affecting the high-power and high-frequency operations was also analyzed by subjecting the HEMT active device regions to the progressive time-temperature annealing cycles. Our suggested model can also provide a functional process window to control the extent of 2D Electron mobility in the AlGaN/GaN HEMT devices undergoing a full cycle of thermal impact i-e from a desirable conductive region to a highly compensated one. The work carried out in this study is very important for the semiconductor process engineering and have ramifications for device engineers.

CHAPTER 01
INTRODUCTION

1.1: Introduction:

The High Electron Mobility Transistor (HEMT) is a kind of field effect transistor that the Japanese invented and successfully commercialized [2]. According to semiconductor theory, the semiconductor layer needs to be doped with n-type impurities to generate electrons in the layer. However, this procedure causes the electrons to slow down because they end up colliding with the impurities residing in the same region that were used to generate them in the first place [2]. HEMT is a smart device that was designed to resolve this contradiction. HEMT accomplishes this by using high mobility electrons generated using the heterojunction of a highly doped n-type AlGaN thin layer and non-doped GaN layer[2]. The electrons generated in n-type AlGaN drop completely into the next GaN layer to form a depleted AlGaN layer, because the hetero-junction created by different band-gap material forms a steep canyon in the GaAs side where the electrons can move quickly without colliding with any impurities[2].

HEMT is a superior device for building a low noise amplifier at a high frequency such as 12GHz[3] already nineteen years have passed since HEMT as invented. HEMT is now widely used as an extremely low noise device in terrestrial and space telecommunications systems, radio telescopes in the area o astronomy, Direct Broadcasting Satellite television (DBS) receivers and a car navigation receiver[3].

We used the HEMT of AlGaN/GaN on the basis of Gallium nitride (GaN) HEMTs excel over competing technology for high power, high frequency applications [1]. GaN HEMTs have an order of magnitude higher power density and higher efficiency over silicon (Si) and gallium arsenide (GaAs) transistors, allowing a ten time size reduction for the same output power, while simultaneously saving material cost [1]. The wide band gap (3.4 eV) allows for rugged high voltage, high-temperature application extensively covering both commercial and military markets[1].

AlGaN/GaN HEMTs with varying source-gate spacing are usually fabricated using a standard technology process developed in various labs. HEMTs are then characterized by their DC, I-V, C-V characteristics, Hall measurements, and high frequency (HF) measurements[4]. A hydrogen silsesquioxane (HSQ)/polymethyl methacrylate (PMMA) T-Gate process is in practice to increase the f_t and f_{max} of the next generation HEMTs. Ohmic contacts with improved morphology and line edge definition after annealing are also traditionally checked for such devices [4].

1.2: Introduction to This Work:

The aim of suggested project as to

I. Study the concept of implantation modeling of III-V based HEMT structure for robust millimeter wave application.
II. Review the experimental procedure.
III. Perform the Monte-Carlo simulation on industrial trade off simulator "stopping and Range of Ions in Matter (SRIM)" [1].

IV. Calculate the power and frequency co-relation with damage.
Monte-Carlo simulation has been performed in order to optimize the implant parameters like ion species, does, damage, energy, angle of incident of devices. This in turn has provided a novel assessment tool to effectively optimize the process design for such devices for application in next generation devices.

1.3: Simulations:

International simulation package, naming trade-off IBM's "Stopping and range of Ions in Matter (SRIM) [1] is used in this work. In this package different input parameter can be analyzed and set in order to achieve required doping profiles. In general by changing the value of each input parameter such as energy, fluency (does) and angle of incident of incident of beam simulation plots can be achieved showing various output parameters of the implantation [1].
By SRIM 2008; the output parameters are collision plots in the form of longitudinal and lateral directions, ion distribution, lateral distribution, ionization, phonons, and energy to recoil and vacancy produce in terms of lateral events. Parameters can be set to obtain certain requirement such as specific depth and damage attain by implantation in HEMT test structure [1]. Matlab was used for plotting the graphs.

1.4 Research Methodology:

In the proposed study, we review the available literature, both from the physical understanding and sample preparation point of view. Then, SRIM Monte-Carlo simulations are performed to optimize the process scheme for appropriate

sample fabrication by choosing the efficient parameters for AlGaN/GaN based HEMT. These conditions include the appropriate ion species, does, angle of implantation; our proposed scheme is then compared with the existing ones in the literature because the specimen structure is intentionally chosen to be the one already tested in literature and commercially. Our results are subsequently discussed in detail.

1.5 Outlines of the Thesis:

This thesis is formatted in such a way that first chapter describes a brief introduction to this work and the sequence of the report. Second chapter reviews the background of related literature that is involved directly or indirectly in this thesis work. In chapter three experimental techniques are discussed that are being used in industry for the HEMT III-V devices similar to our test structure. Chapter four describes detailed methodology adopted as well as the discussion on the results obtained using the SRIM model.

CHAPTER 02

LITERATURE REVIEW

2.1: Introduction:

In this section, the work done by the researchers related to the broader scope of our problem focused on the design and fabrication of III-N-V HEMT structures is being summarized. The findings are tabulated as follows:

Table 1. *Literature Review*

Title (Reviewed Article)	**(Major Findings)**	**Reference**
MOCVD grown AlGaN/AIN/GaN HEMT structure with compositionally step-graded AlGaN barrier layer [62].	• Unintentionally doped AlGaN/AIN/GaN HEMT structure [62]. • Sapphire Substrate [62]. • Algae barrier using MOCVD [62]. • 2DEG Mobility = 1600 Volt-centimeter/square [62]. • Avg sheet resistance = 318Ω/square [62]. • RMS Roughness = 0.199nm [62]. • Higher electrical performance [62].	62
Oxygen Ion Implantation Isolation Planar Process for AIGaN/GaN HEMTs [63].	• Multienergy oxygen ion implantation process [63]. • AlGaN/GaN HEMT [63]. • Process isolated HEMT found gate lag and drain free [63]. • Max power output density of 5.3 W/mm at Vgs= -4V, Vds=50V [63].	63

	• Max power added efficiency = 51.5% at Vgs = -4V & Vds= 30V at 3GHz [63].	
AlGaN/GaN High Electron Mobility Transistor Structure Design and Effects on Electrical Properties [64].	• Strain induced polarization effects in AlGaN/GaN Hetrostructure[64] • Si dopant ion in the lattice [64]. • Contraction of the wurtzite unit cell [64]. • Strain in doped AlGaN/GaN hetrostructure[64]. • Strain can create additional source of charge [64].	64
ION IMPLANTATION OF Si, Mg AND C INTO A10.,2G-.88N[65]	• Mg and C were implanted in undoped semi-insulating layers of Al, Ga, N with x=0.12[65]. • Activation of implanted Si occurred after annealing at 1140 C in ammonia [65]. • Anneal at 800 C in nitrogen [65].	65
Study of fluorine bombardment on the electrical properties of AlGaN/GaN heterostructures[66].	• Effects of fluorine ion bombardment on the channel transport properties of AlGaN/GaN heterostructures[66]. • Hall mobility and sheet electron concentration for the two-dimensional electron gas showed strong dependence on bombardment duration and post bombardment annealing [66]. • Diffusion followed by accumulation of the ions at the heterointerface[66].	66
Undoped AlGaN / GaN HEMTs for Microwave Power Amplification [67].	• Undoped AlGaN/GaN structures used to fabricate (HEMTs)[67]. • (3D) nonlinear thermal simulations [67]. • Temperature rise from heat dissipation in various geometries	67

	determined [67].	
High-Power Microwave GaN/AlGaN HEMT's on Semi-Insulting Silicon Carbide Substrates [68].	• Record performance of high-power GaN/A10:14-Ga0:86N HEMT fabricated [68].	68
Enhancement-mode AlGaN/GaN HEMTs Fabricated by Standard Fluorine Ion Implantation [69].	• Fabrication technology of enhancement-mode AlGaN/GaN HEMT [69]. • Standard fluorine ion implantation [69].	69
Ion Beam Application to Next Generation Micro-and Nanoelectronics: A Brief overview [70].	• The article provides a brief overview on recent advancement of ion beam application [70].	70

The improvement of ohmic contact of Ti/Al/Ni/Au to AlGaN/GaN HEMT by multi-step annealing method[71]	• A multi-step rapid thermal annealing process of Ti/Al/Ni/Au was investigated for Ohmic contact of AlGaN/GaN HEMT [71]. • The AES measurements showed that the limitation in diffusion of Au and out diffusion of Al were account for the surface morphology improvement and the surface Fermi level towards the conduction-band edge resulted in a lower specific contact resistance [71].	71

Post-annealing effects on device performance Of AlGaN/GaN HFETs [72].	• The effects of post-annealing on DC, RF, and power performances of AlGaN/GaN HEMTs with a gate-length of0.3 lm were investigated [72]. • The results show that the post-annealing technique can improve the device breakdown voltage and device uniformity, reduce the trapping centers on AlGaN surface and/or GaN buffer layer after the post-annealing, and adjust the device threshold voltage [72].	72
Stability of submicron AlGaN/GaN HEMT devices irradiated by gamma rays [73].	• Stability of submicron AlGaN/GaN HEMT devices irradiated by gamma rays[73]	73
Effect of metal ion implantation on thermal instability Of diamond-like carbon films [74].	• Investigated the effects of ion species and doses on carbon related bonding property such as the ratio of sp3 carbon to sp2 phase, the chemical composition and tribological properties of the DLC films [74].	74
Effect of plasma immersion ion implantation on the thermal stability of diffusion barrier layers [75].	• Plasma immersion ion implantation technique has been used to synthesize titanium nitride and tantalum nitride layer to acts as diffusion barrier against copper diffusion investigate the effect of annealing [75].	75
Effects of Ar-ion implantation and thermal treatment on magnetic properties of Co/Pd	• Volume and surface anisotropies of Co/Pd multilayers have been studied by ferromagnetic resonance (FMR) and vibrating sample magnetometer (VSM)[76]	76

multilayers: a ferromagnetic Resonance study [76].	• Measurements for different layer thicknesses and as a function of thermal treatment and before and after ion implantation [76].	
Temperature-Independent High Voltage Reference Design in Silicon-on-Insulator CMOS Technology [77].	• Temperature independence for voltage reference circuits designed in Silicon-on-Insulator CMOS technology [77]. • This paper focuses on unique aspects of design in this process, using a voltage reference as a Vehicle [77].	77
The AlInAs-GaInAs HEMT for Microwave and Millimeter-Wave Applications[78]	• This paper reviews the status of lattice-matched and pseudomorphic AlInAs-GaInAs HEMTs grown on InP substrates [78].	78

CHAPTER 03

EXPERIMENTAL TECHNIQUES: FABRICATION AND PROCESSING OF PRE-AND POST-SIMULATED DEVICES

3.1 Ion Implantation

3.1.1 Introduction

Ion Implantation is a method of introducing impurities in to a substrate that does not use heat, in other words, we can say that, it is a non thermal method [5]. Ions are energized, the energized Ion then enters the crystal lattice where they collide with the silicon atoms and finally they come to rest. The energy required to ionize these ions may range from a few KeVs to MeVs, depending on the weight of the ion and the nature of the substrate, the possible depth attainable from this method may range from Ion 10 to 1000 mm [6].

The acceleration we give to the ions decides the depth of the dopant atoms and to control the concentration of the dopant we have to mention the ion keeping in view, how shallow or deep one wants to implant[5]. Ion implantation is very useful as it has the ability to control with precision, doping level and the depth of implantation, by varying of the energy and amount of ions [5].

When the method of ion implantation was developed, it was just seen as a method of introducing imparities in to senior conductors, but the experiment proved that its ability and accuracy of controlling the dopant concentration implantation depth makes it the choice procedure in comparison with the other procedures such as diffusion etc [5]. It also has the ability to work at room

temperature, and the results attained are also very accurate in terms of uniformity and cleanliness [5].

Ion implantation ahs attained the position of a standard technique for introducing imparities in to a semiconductor [13]. In this method positive ion are produced, which are then accelerated through a controlled potential to the target substrate[5]. In comparison to diffusion, it has better controllability and it has the ability to implant using a master[5]. It has become very popular in microelectronics. In industrial products on, it is widely used, especially in the field of IC design. One example may be cited in the production of CMOS devices[5].

3.1.2 Stopping and Range of Ions:

An ion thrown with some energy in to a target atom, loses its energy by colliding with electrons and the nuclei with in the target atoms[5]. These ions come to rest by these two mechanisms i.e. collision with the electron or collision with the nuclei. In the nuclear collision the kinetic energy in transferred to the target atom, while the bombarding ion is deviated from its trajectory considerably[5]. At higher incident energies the electronic factor is dominant in the stopping of the ion, while the nuclear factor is negligible[5]. In case of electronic collision, the energy is transferred to the electron and there is negligible diversion in the trajectory of the bombarding ion. The total stopping power may be described with the help of mathematical expression below[16]:.

$$S = \left(\frac{dE}{dx}\right)n + \left(\frac{dE}{dx}\right)e \qquad (3.1)$$

Where dE/dx is the energy loss per unit path of the ion. Using this mathematical expression and finding the stopping power, and integrating it we can

also find out the distance that ion will travel inside the target, before losing it's energy and finally coming to rest. The typical energies used in an implantation are from 10eV to 200 eV [5].

Both nuclear and electronic mechanisms contribute towards the energy loss of the incident ion inside the target atom. As the number of ions in an implantation are very large, usually larger than to 12 ions/cm2 [25]. It is more appropriate to consider that [Rp][26] is the average depth of the implanted ions.

Ion concentration n(x) as a function of depth can be described with the help of following mathematical expression[15].

$$N(x) = n \exp\left[\frac{-(x-RP)^2}{2\sigma^2 P}\right] \tag{3.2}$$

The above expression represents a mathematical model: the real distribution may differ from it. To take in to the account these differences, skewness [16], kurtosis [16], and other parameters may be considered.

In case the target is a crystalline solid. The impinging ions move through the directions where the chances of collision is minimum e.g. atoms rows or planes [5]. By doing this, the ions can travel deeper in to the target rest there. This phenomenon is called channeling and it is responsible for the asymmetrical implant distribution inside the target [5].

3.1.3: Ion Induced Damage:

Despite of many advantages, such as introduction of an accurate dose of impurity atoms to be placed at a controlled distance from the surface of the substrate. The disadvantage is the introduction of damage. High energy ions displace the atoms in the substrate from their position in the crystal structure. In

addition to that only a few implanted impurity atoms and up in the correct lattice site.

As described the implanted ion lever energy in two way i.e. electronic collision or nuclear collision. It reaches a resting plant producing ionization or electronic excitation and resultantly thermal or photonic emission. The effect is a little different in case of nuclear scattering require. It is quite easy to produce displacement of the target action, as the binding energy of the lattice is just 10-20V [18]. The displaced atom and the ion still have sufficient energy to displace further atom and form so called cascades [5]. The result is missing atom in the lattice position called vacancies [5]. These vacancies can be filled by the implanted impurity atoms [5].

If heavy ion is implanted in to lighter targets denser cascades are formed and the defect structure so produced is also quite different from the other extreme [5]. In this case when the heavy ion strikes the surface of silicon, it deflects and continues in to crystal lattice along with the recoil atom [5]. The ion and the recoil atom have enough energy to produce more displacements [5]. The ion energy shared by ions and recoil atoms produce cylindrical cascades with axis along with path of the ion [5].

The ion energy determines the amount of damage produced [5]. If the ion energy remains constant heavier ion will produce more damage than the lighter ion [5].

3.2 ANNEALING

3.2.1 Introduction:

After implantation annealing is required, in order to repair the damage and to put the dopant atoms on the vacancies, where they can be electrically active [5]. But while performing there true tasks i.e. repairing the damage and electrically activating the dopant atoms, care needs to be taken that nature of the implant is not disturbed i.e. shallow implant remains shallow[5].

The important or the critical factors in annealing are the temperature maintained and the time for which the implanted sample is exposed to that temperature [5]. This is also called annealing cycle determines the sitting of impurities atom in the host lattice which in turn determines the resistivity, conductance and other properties of the material[5].

For amorphous layer the electrical activation of dopant atoms is a bit different. For amorphous layer electrical activation takes place when impurities are incorporated in to lattice sites during recrystallization [5]. When the doping atom moves according to a fixed dopant gradient in to a semi conductor it is called diffusion [5]. It takes place, either intentionally or parasitically, during any high temperature proceeding step [5]. In modern days ultra shallow junction are required in the semi conductor technology, therefore, diffusion is mostly seen as a parasitic effect of ion implantation or oxidation step, which are performed at high temperatures[5]. But still diffusion has many applications like well formation in CMOS technology [5]. The diffuse ability of different dopant species are different [5]. Oxidation enhances diffusion while nitridation retards it because it produces point defects on the surface [5]. These point defects as well as the implantation induced point defects can strongly influence the diffusivity, because they

introduce complex diffusion mechanism like transient enhanced diffusion [20]. At high concentration levels, the dopant atoms may form non mobile clusters, which will affect adversely the average diffusivity [5]. All diffusion mechanisms must be controlled exactly during the manufacturing of a semiconductor device, as the re-distribution of dopant may bring undesirable changes in the electrical properties of the device [5]. When the clustering and precipitation occurs in case of dopant concentration above solid solubility limit (SSL), a portion of the diffused atoms appears as electrically inactive at room temperature [21]. This effect need to be considered during simulation [5].

3.2.1 Types of Annealing:

Annealing can be of various types like laser, furnace, microwave, incandescent lamp [5]. The most important of them all is rapid thermal annealing (RTA) or rapid thermal processing (RTP). RTA/RTP is a process of short duration, satisfying certain parameters [5]. It may contain any one or more types of annealing discussed above. Here RTA/RTP is discussed keeping in view all the types of annealing [5].

3.2.1.1 Furnace Annealing:

A bell Jar method for annealing implant motions was developed at high temperature Engineering [5]. Further improvement was made recently with an emissive compensating temperature measurement scheme [5]. The wafer is elevated on a support platform, in to high temperature zone with a vertical temperature gradient [5]. The highest temperature of about 200C above the desired process temperature is set at the top of the bell Jar [5]. Due to the comparatively

weak sensitivity of wafer temperature to wafer remissibly within an almost black body environment at high temperature, this has become a visible method for open loop operation in some production work [5].

Elevator motion is fast enough to produce to produce thermal spiking with 0.5s dwell time 2C short of peat temperature [5]. Best results have been achieved with pyrometer focused on the back side of the wafer under closed loop temperature control, in terms of process reproductively and uniformity. In case of bell jar system the pyrometer detect is the electric flux emitted by the wafer and measure the resultant emissivity of the wafer. Emissivity E is defined as the ratio of thermal emission from the wafer with respect to the thermal emission of the black body at the same temperature [23]. The wafer length at which the pyrometer operates is about 0.95 um. Which is above the silicon band gap optical transmission on through the wafer can be neglected. Application of law of conservation of energy and kick off law we arrive at

$$E = 1-R \qquad (3.3)$$

This expression is used to compute emissivity from reflectivity, R [5]. The reflectivity is determined in a multistep process, first geometrical and background reflection factor are mapped, a function of evaluator is added as height then bidirectional reflection signals are normalized to a separate existed measurement of R at room temperature using hemispherical illumination. Wafer temperature is finally computed using plant radiation law and gauge factor for detector sensitivity [5].

3.2.2.2 Rapid Thermal Annealing (RTA):

RTA is the most popular method of activating the dopant atoms after implantation [5]. In this method, system processes one wafer at a time [5]. The system configuration may be different for each process, but for shallow junction creation we have heat the wafer at ultra high temperatures ranging from 900C to 1100 for a few seconds or less [5]. The time for which wafer remains at peak temperature is called soak time [5]. Ramp up rate of up to 40C-400C can be achieved [5]. One of the popular types of RTA is a spike anneal [5]. This involves ramping up the wafer to peak temperature for a few milliseconds and then ramping it down [5]. Minimum hold time at peak temperature and ramp up rate is dependent on system configuration [5]. Two of the most common configurations are hot walled system and lamp based system [5]. Here the wafer is ramped up to 600 – 700C held at that temperature for a few records, before being ramped up to peak temperature [5]. This reduces the stress in the wafer but increases the thermal budget [5]. The wafer cools down through radiative cooling from the surface of the wafer and conduction through the wafer holder. In the lamp based system, the cooling rate is observed to be 70C/sec while in hot walled system it is 60C [22]. The cooling down rate also contributes toward increasing the thermal budget [5]. Hot walled system is mostly used in current mainstream IC processing [5]. In RTP only the wafer is heated and cooled from the processing temperature [5]. The walls of the chamber are water cooled [5]. The windows are air or water cooled, therefore, the process steps may only take ten second for completion [5].

Various arrangement have been designed in order to heat the wafer in-visible light or ultraviolet light or both [5]. Light passes from lamp array source to the wafer using the upper widow [5]. The lower window may be used for remote

temperature measurements of the wafer or ultraviolet treatment of the wafer. Lamp array typically requires the power of up to several tens of KW [22].

Advantages of RTP include lower thermal budget, a shorter duration of high temperature processing time, and better process repeatability [5]. Since the wafer is far from equilibrium from it's surrounding the problem of non uniformity of temperature throughout the wafer is greater than in case of hot oven processing [5]. During I.C. manufacturing silicon wafer under goes various processes at high temperature, various atmospheric conditions, and high level of heat power [5]. Research is still going on for accurate control mechanisms to provide real time monitoring [5].

One of the major problem areas in this research is the non uniformity of temperature all over the wafer [5]. A mean uniform temperature is required to be maintained all over the wafer [5].

It is important to monitor the temperature all over the wafer using pyrometer located outside the chamber, double-pars infrared transmission and multiwave imaging pyrometer are some of the techniques applied for doing so [5].

3.3 Displacement Energy:

The energy required by the recoil to overcome the target lattice force and to move away from its original site more than one atomic spacing [5]. If the recoiling atom does not move more than one atomic spacing away from its original site, it is assumed that it will go back to its original site and will give up the recoil energy into phonons [5]... Typically the value of displacement energy is about 15eV for semiconductors and 25eV for metals. For granite materials this value may be from 2-5 eV [5].

3.4 Binding Energy due Surface Kinetics:

This is the energy that must be overcome by the target ion in order to leave the surface of the target [5]. This energy should not be seen as only the chemical binding energy between the atoms, rather it includes all the surface non linearity e.g. those produced by radiation damage, surface relaxation, surface etc[5].

3.5 Binding Energy Due to Lattice Kinetics:

The energy that the recoil target atom must lose at the time of leaving the lattice site and recoiling in the target. Its typical value ranges between 1 to 3eV [5]. For most compounds this value is not known [5]. Typical assumption is that this energy goes in to phonons. This energy is also very significant in computing the sputtering yield [5].

3.6 RESISTIVITY AND HALL MEASUREMENTS

The Hall Effect technique is well known to draw conclusive evidence on the conductivity type of the semiconductors. This also provides a substantial information of sheet resistivity (R_s), mobility (μ_s) and sheet carrier concentration (n_s) governing the following expression deduced in literature [60 and references therein] and widely used in the industry.

$$n_s = IB/q|V_H| \qquad [60]. \qquad (3.4)$$

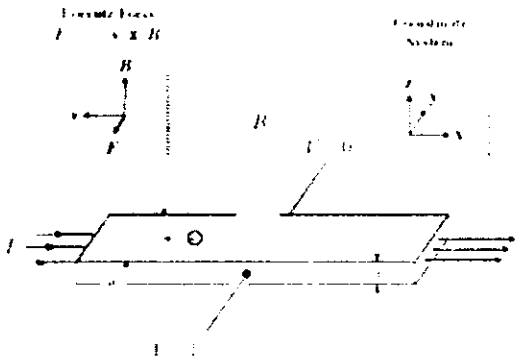

Fig: 1*: An* n*-type, bar-shaped semiconductor* [60]

$$\mu = |V_H|/R_S IB = 1/(qn_S R_S). \quad [60] \qquad (3.5)$$

If the conducting layer thickness d is known, one can determine the bulk resistivity ($\rho = R_S d$) and the bulk density ($n = n_S/d$) [60 and references therein]. I, B, q, VH in these expressions are current, applied magnetic field, charge and Hall voltage.

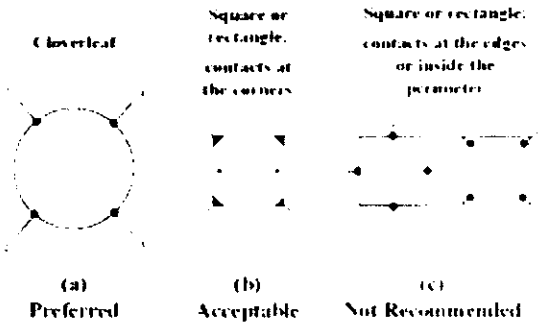

Fig 2: *Sample Geometry* [60]

It is preferable to fabricate samples from thin plates of the semiconductor material and to adopt a suitable geometry, as illustrated in Fig. 3.2[60]. A schematic of contact measurement during Hall and resistivity measurements using electrical point contacts is shown in Fig3.3 below. The resistivity is dependent on the quality of the contacts and the uniform dc voltage measured between contacts.

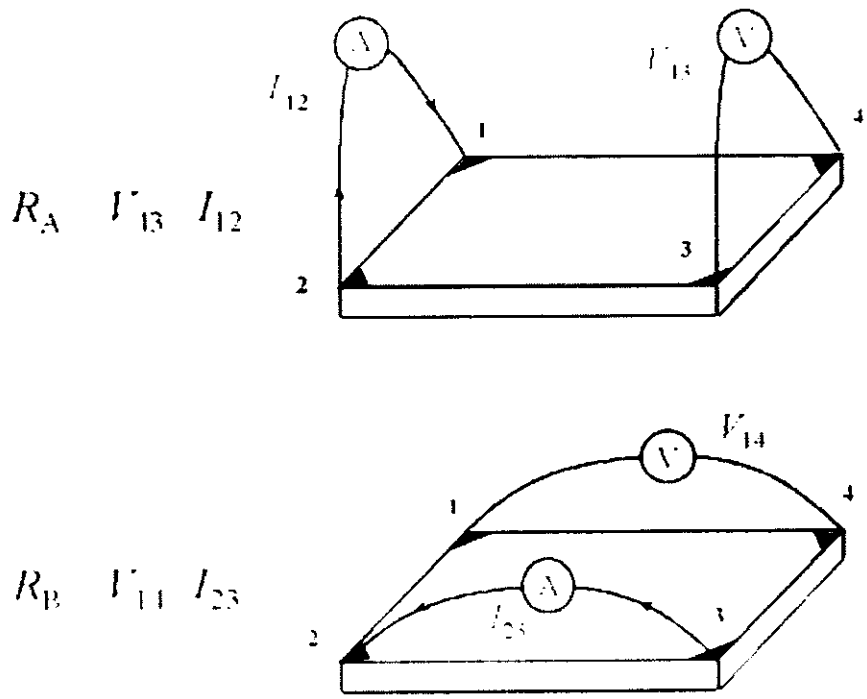

Fig 3: *Definitions for Resistivity Measurements* [60]

Yield the following eight values of resistance, all of which must be positive:

$$R_{21,34} = V_{34}/I_{21},\ R_{12,43} = V_{43}/I_{12},$$
$$R_{32,41} = V_{41}/I_{32},\ R_{23,14} = V_{14}/I_{23},$$
$$R_{43,12} = V_{12}/I_{43},\ R_{34,21} = V_{21}/I_{34},$$
$$R_{14,23} = V_{23}/I_{14},\ R_{41,32} = V_{32}/I_{41}. \qquad (3.6)$$

The sources of errors in Hall measurements are efficiency of contacts, geometry of the sample and current source, which is reasonably acceptable if a cumulative source is less than 5% [60].

3.7 SRIM (Stopping and Range Of Ion in Matter)

3.7.1 Introduction:

TRIM is a group of programs that two things namely stopping and range of ions (10eV – 2GeV/amu) in to matter using a quantum mechanical treatment of

ion-atom collision [1]. For this introduction of SRIM moving atom will be referred to as ion while the target atoms will be called atoms [1]. Very efficient statistical algorithms are used which allow the ion to jump between calculated collision, and then average is taken for the collision results over the intervening gap [1].

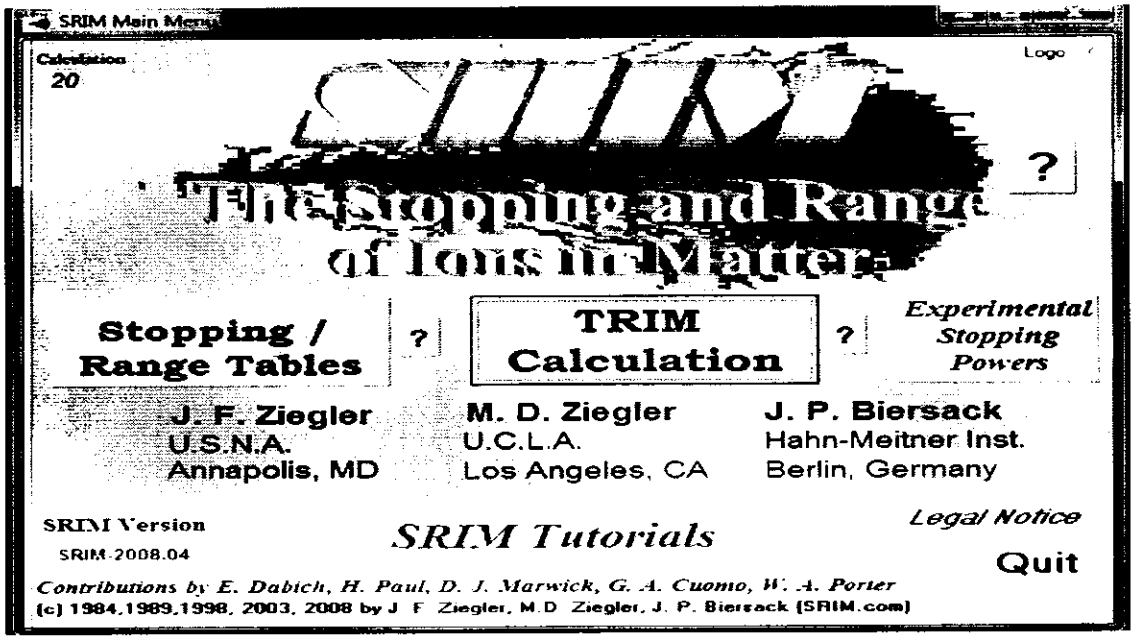

Fig .4: SRIM Setup window

The collision between ion and atoms is screened coulomb collision, which includes both exchange and correlation interaction between the overlapping electron shells [1]. The long range intention of ion result in electron excitation and plasmons within the target [1]. For its description, a description of the targets collective electronic structure and int erionic bond structure is included in the calculation set up [1]. The concept of effective charge is used to describe the charge state of ion within the target [1]. The concept of effective charge state of ion within the target. The concept of effective charge comprises of a velocity dependent charge state and long range screening due to the collective electron sea of target [1]. TRIM ahs the capacity to accept complex targets made up of compound materials with up to eight layers [1]. It will calculate not only the final

3D distribution of the ions, but also the kinetic phenomena associated with the target damage, ion energy ions, sputtering ionization and phonon production[1]. The target cascades can also be taken in to account if required, in fact a great deal of information about the target cascades can be made available [1]. The programs can be stopped and resumed at any time. Plots of calculation can also be saved and displayed at the time of choice [1].

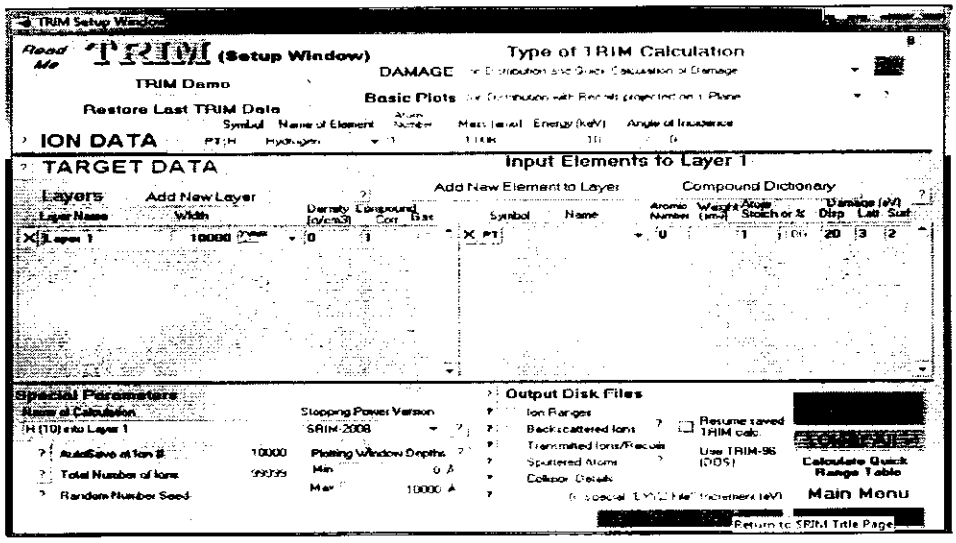

Fig 5: TRIM Setup window

TRIM is contained in the programs called SRIM (The Stopping and Range of Ions in Matter) [1]. It can be accessed from its Title page by pressing the button marked TRIM [1].

3.7.2 Some Concepts about SRIM Calculations

Ion distribution and quick calculation of damage is a type of calculation [1]. These types of calculation is applied when we are not worried about the target damage, or sputtering quick statistical estimates regarding the damage are made union kinship – Pease formalism [1]. The data calculated will be calculated accurately using this calculation [1]. The end or final distribution of ions in the target.

transmitted and back scattered ions, ionization energy loss by the ion into the target, Energy transferred to recoil atoms [1].

This quick damage calculation should be used if you don't give any significant importance to the details of target damage or sputtering [1]. The damage calculated in this type of calculation will be the quick statistical estimates based on the Kin chin – Pease formalism [1]. The under mentioned data will be calculated correctly: Final distribution of ions in the target. Ionization energy loss by the ion into the target. Energy transferred to recoil atoms. Backscattered Ions and Transmitted Ions [1]. You will get similar ion ranges results as when you use the Full Damage Cascade option below. because the random number generator for the ions is different from that used for the recoils. This is useful to compare calculations [1].

In detailed damage calculation every recoiling atom is followed until the time that it losses it's energy below the lowest displacement energy of any of the target atom [1]. The only exceptional case is of massive cascades exceeding 20,000 atoms [1]. The reason for this exception is that TRIM memory at this point is furnished TRIM stops the calculations and given an error message [1]. The number of recoiling atom in a single cascade has exceeded the limit of 20.000[1].

The requirement for monolayer collision step is the ion to have a collision in each monolayer of the target [1]. Every collision is calculated without any approximation as the possibility of the use of free flight path is omitted [1]. The result will be the same averaged quantities like mean range, ionization, damage, etc, but the calculation will take far too long to complete special calculation like sputtering require this type of calculation to generate data on every possible collision in the file COLLISION.Txt[1].

The calculation of surface sputtering requires monolayer collision steps [1]. That is the ion must have a collision in each monolayer of the target [1]. Special

plots are available which allow close examination of small variations of the surface binding energy on the sputtering yield [1]. Surface binding energy is at the heart of sputtering [1]. This parameter is very difficult to estimate. Heat sublimation values provided by TRIM provide a good estimate of surface binding energy [1].

Any ion can be chosen from the periodic table, or alternatively the symbol of the chosen ion can be written e.g. H for hydrogen. He for Helium, and so on [1]. Mass suggested by the TRIM is the mars of the most natural weight [1]. However any mars can be entered but the units will be KeV in this case [1]. The range of acceptable values is from 10KeV to 10GeV/am [1]. TRIM does not have the capability to analyze nuclear reactions [1]. Therefore the inelastic energy losses above 5MeV/amu are not included in the TRIM calculations [1].

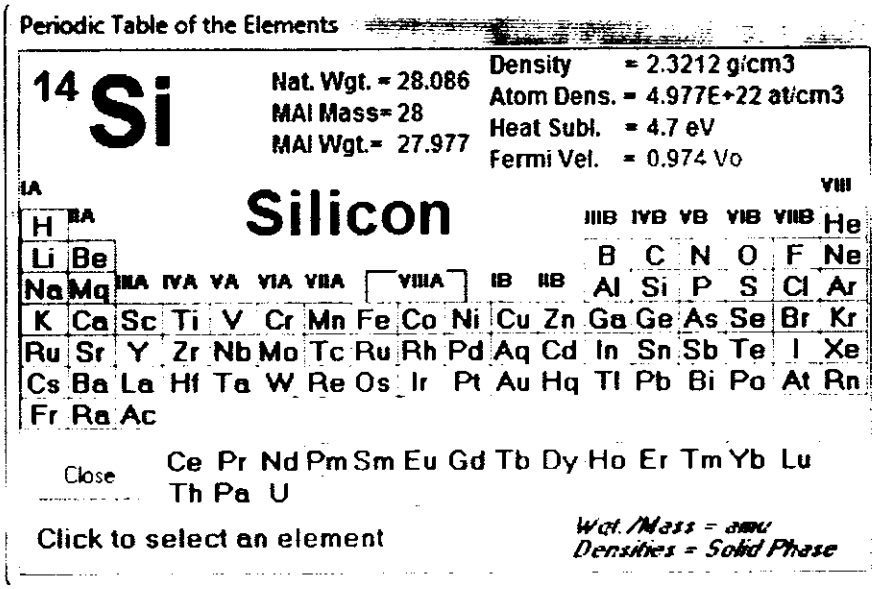

Fig 6: The Periodic Table

We can also give the angle of incidence of the ion on the surface of the target [1]. Zero degree is taken to be perpendicular to the surface of the target [1]. The angle

of incidence may be changed within the range of 0 to 89 degrees in the XY plane [1].

Gaseous target are considered different from solid targets is TRIM [1]. Target can also be mixed i.e. gas and solid [1]. If a target contain normal as in target e.g. oxygen in solid form in a quartz target, it should be declared and will be treated as solid [1].

The user can input the various target elements in the same way, he inputs the ion [1]. The simple way of doing so is by pressing the pt button and choosing it the element of choice from the periodic table up to twelve target elements can be added per layer [1]. TRIM follow the mixing of layers by ion beam, which results in the formation of cascades [1]. For example. If a user wants to follow silicon atoms from a surface layer of SiO2, they can specify silicon twice once for the substrate and once for the surface [1]. TRIM will keep separate record for both Si atoms and various analytic plots can be used to distinguish the two silicon atoms [1].

TRIM also has a repository for commonly used compounds, in which basic information like stoichiometry, density, bonding information, provided [1]? This table can be used and most for the target input steps can be avoided [1].

Once you choose a target element you will have to choose its thickness [1]. The default unit for choosing the thickness is angstrom, but you can also choose in micrometer, manometer, millimeter, we will also have to choose the ratio the ratio of a certain element in a target compound e.g. for Silicon dioxide, Silicon is One and oxygen is two [1].

Each layer has a density (units=g/cm3) [1]. TRIM guesses at densities, which is based on a mixture of elemental target densities weighted by their relative stoichiometry [27]. However, one should be careful to check the reasonability of the density guessed in this manner [1].

You can always choose the name of your choice for any layer, and the layer will be described in any plot or data using that name [1]. You can choose simple or somewhat descriptive name of your choice, Si, SiO2, Si (33) [1].

TRIM uses the entire target depth to generate the averages like projected range, vacancies/ion etc. but any portion of the target can be enlarged in order to analyze it more closely [1]. This is called Trim's Viewing Window [1]. This is very important consideration for thick targets [1]. The depth window allows the user to expand a small region in the target to extract finer details from it [1]. One of the examples of TRIM view window is in TRIM demo called "He (5 MeV) in a Gas Ionization Detector" where although the target is 50mm deep but the view window is set at 40mm-50mm to have a detailed view of the He end of range ions for both data files and plots [1]. This window is divided in to 100 depth bins by the TRIM in which it stores average data for the calculations, a couple of examples of such data are the energy loss to ionization and the final ion ranges[1].A maximum number of 99,999 ion can be set using this option. a lesser value can also be chosen. This is also possible that the calculation is stopped at a certain point after choosing the default value of 99999. One may wish to stop after a selected number of ions so that different TRIM calculations may be compared. If a TRIM calculation is repeated, every ion will be exactly same as for the previous calculation unless the random number seed is not changed. If the user has requested for a calculation with lesser number of ions he can increase the number of ions after the completion of that calculation by first resuming saved TRIM calculation and then increasing the number of ions [1].

Since TRIM calculations may take days to complete, TRIM automatically saves it at intervals. You may change this number during the calculation. It may range from 1-32000 [1].

Until the random number is not changed, there is no difference in the successive calculation. This random number can be any integer between 1-999999999[1].

CHAPTER 04
EXPERIMENTS, RESULTS AND DISCUSSIONS-I
(THE DESIGN)

4.1 HEMT Structure: AlGaN/GaN Structure

4.1.1 Introduction:

Gallium nitride (GaN) HEMTs excel over competing technology for high power, high frequency applications. GaN HEMTs have an order of magnitude higher power density and higher efficiency over silicon (Si) and gallium arsenide (GaAs) transistors, allowing a ten time size reduction for the same output power, while simultaneously saving material cost. The wide band gap (3.4 eV) allows for rugged high voltage, high-temperature application extensively covering both commercial and military markets [29]. In this study, HEMT Test devices were characterized by their resistivity, Hall and Transconductance measurements.

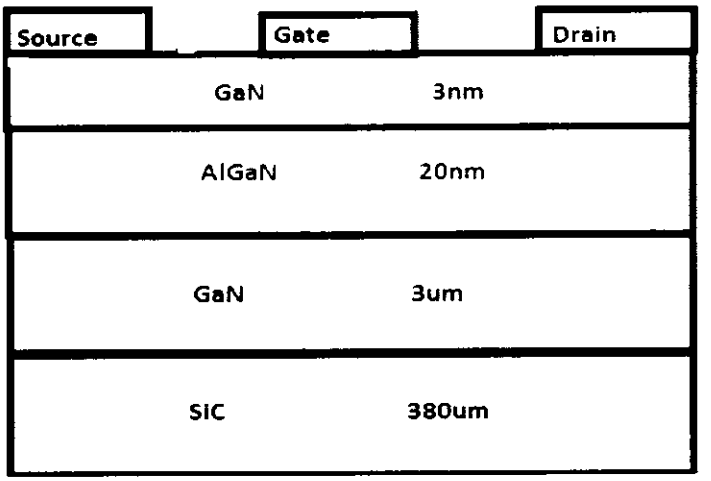

Fig 7: HEMT Structure (Commercially Available Test Device)

4.2 Damage Calculation:

Extensive damage calculations are performed using industrial simulation package (SRIM 2008). The simulation experiments are performed in following manner [5]:

a) In putting the layer device architecture into the simulator.
b) Choosing the input parameters such as ion energy, ion specie, fluency (normalization factor), beam angle, solid solubility limits and ion-matter interaction models.
c) Iterative output graphs normalization.
d) Checking the overall routines with respect to the desired process optimization parameters on one by one basis.
e) Analysis and final selection.

Ion species (He, N, O, F, Cl, Zn, and Si) are simulated in structure with different energies described below for each specie. For each set of ion-energy matrix; the procedure given in section 4.2 is followed on iterative basis so that process may be optimized.

4.2.1 Damage Calculation for Helium

Implanted energies used for Helium are 3.00 MeV, 3.10 MeV, 3.15 MeV and 3.25 MeV. Now Helium ions are implanted in the device structure shown above using these mentioned energies in simulation and a damage profile is obtained for each category, as shown under:

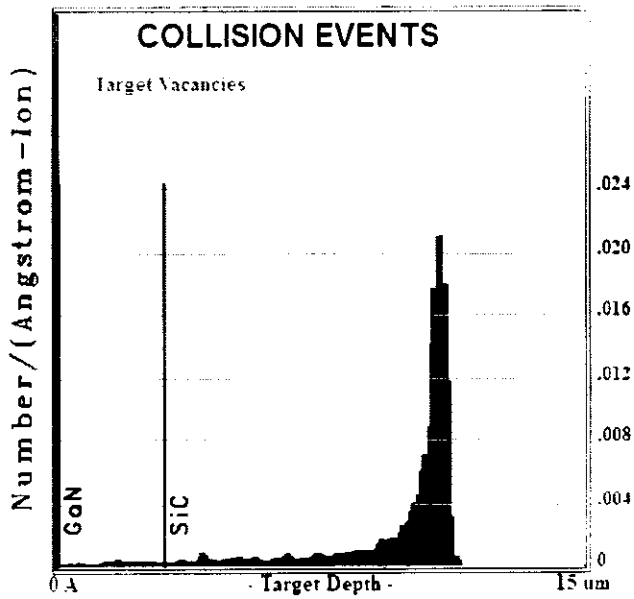

Fig 8: Collision events Helium at 3MeV

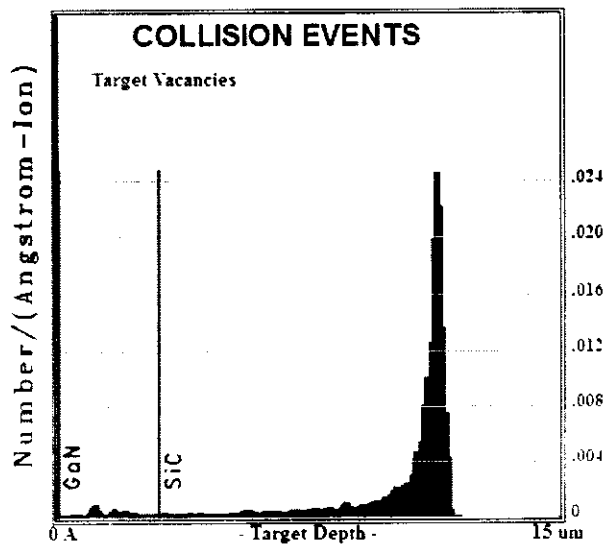

Fig 9: Collision events Helium at 3.1MeV

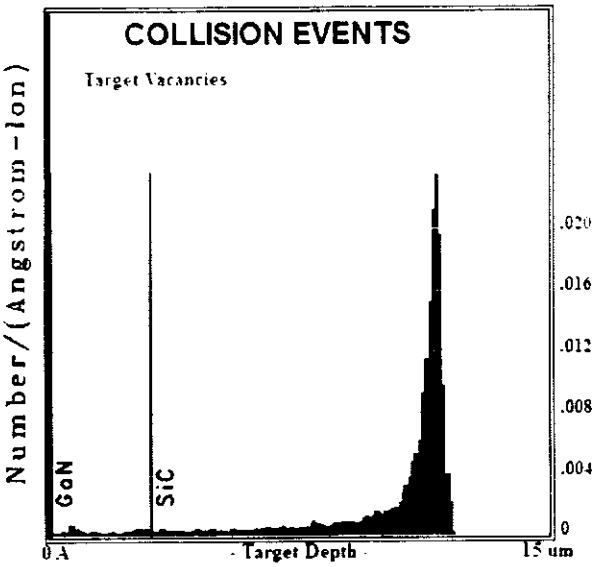

Fig 10: Collision events Helium at 3.15MeV

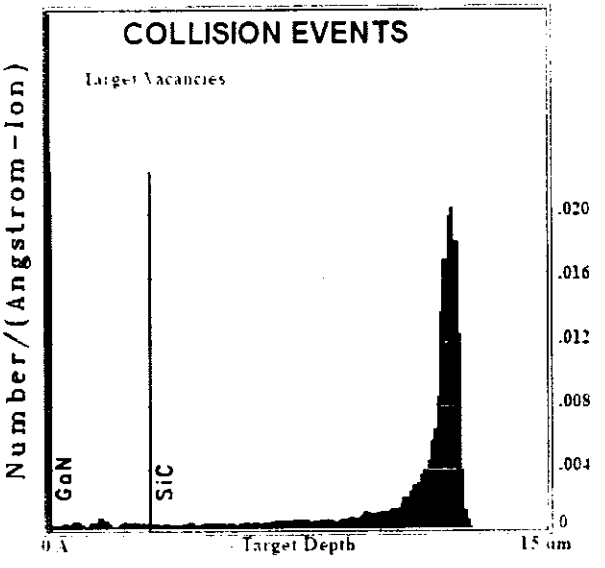

Fig 11: Collision events Helium at 3.25MeV

The above mentioned plots (fig. 4.2-4.5) are generated by SRIM. Each data points are representing damage created by specific energy. As it is shown from the graph that damage created by Helium ion changes as the implanted energy is changed.

Table2 Damage calculation w.r.t. depth attained by Helium ions

Ion Energy (MeV)	Ion Ranges Rp(um)	Extent of Damages (%) (vac/ion/ang)
3.00	10.8	0.0065x100=0.65
3.10	11.2	0.0063x100=0.63
3.15	11.5	0.0059x100-0.59
3.25	12.0	0.0061x100=0.61

.

For other high energies of 3.10 MeV, 3.15 MeV and 3.25 MeV damage created is 0.0063 vac/ion/ang., 0.0059 vac/ion/ang and 0.0061 vac/ion/ang., respectively.

4.2.2. Damage Calculation for Nitrogen

Implanted energies used for Nitrogen are 3.15 MeV, 3.25 MeV, 3.35 MeV and 3.45 MeV. Now Nitrogen ions are implanted in the device structure shown above using these mentioned energies in simulation and a damage profile is obtained for each category, as shown under

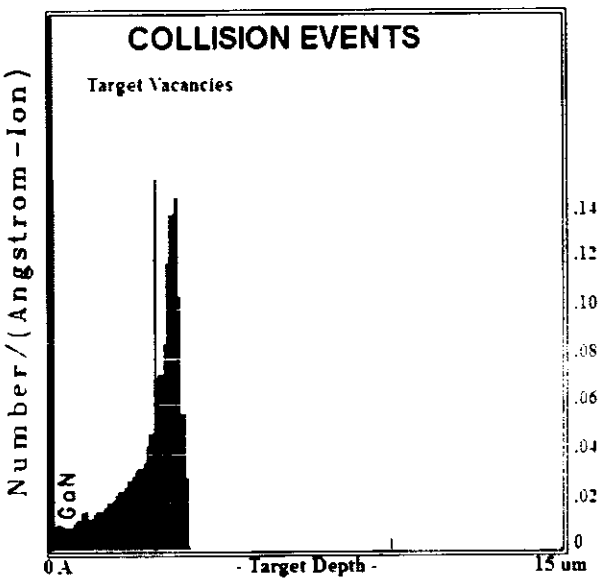

Fig 12: Collision events Nitrogen at 3.15MeV

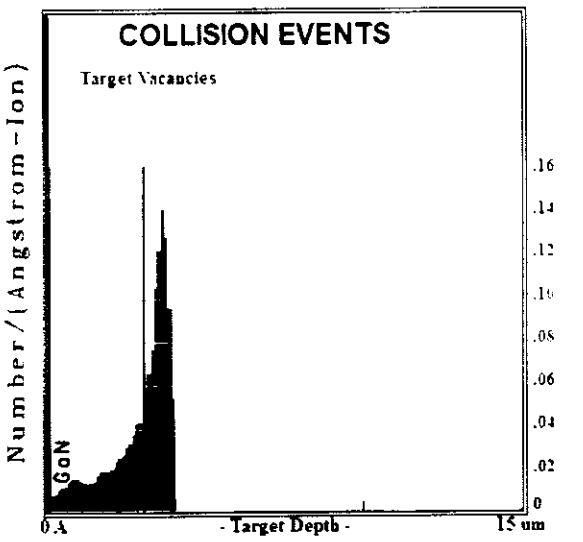

Fig 13: Collision events Nitrogen at 3.25MeV

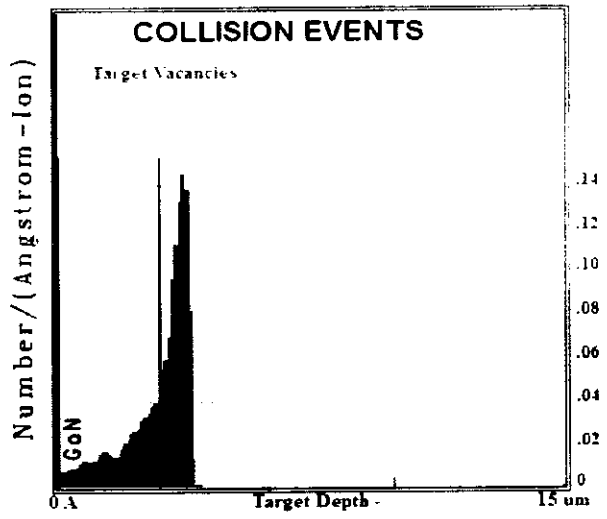

Fig 14: Collision events Nitrogen at 3.35MeV

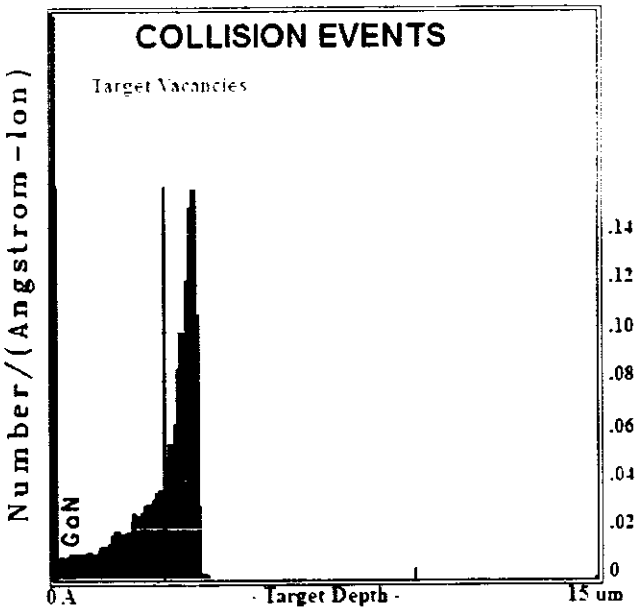

Fig 15: Collision events Nitrogen at 3.45MeV

The above mentioned plots (fig 4.6-4.19) are generated by SRIM 2008. Each data point is representing damage crated by specific energy. For the ion energy of 3.15 MeV maximum damage created is 0.0181 vac/ion/ang and this damage is crated at depth of 36000 A in the structure

Table 3: Table showing damage calculation w.r.t. depth attained by Nitrogen ions

Ion Energy (MeV)	Ion Ranges Rp(um)	Extent of Damages (%) (Vac/ion/ang)
3.15	3.61	0.0181x100=1.81
3.25	3.67	0.0819x100=1.89
3.35	3.71	0.0184x100=1.84
3.45	3.78	0.0240x100=2.40

For other high energies of 3.25MeV, 3.35MeV and 3.45MeV damage created is 0.08189 vac/ion/ang.0.0184 vac/ion/ang. And 0.0240 vac/ion/ang. Respectively.

4.2.3 Damage Calculation for Oxygen

Implanted energies used for Oxygen are 3.15 MeV, 3.30 MeV, 3.40 MeV and 3.55 MeV. Now Oxygen ion are implanted in the device structure shown above using these mentioned energies in simulation and a damage profile is obtained for each category, as shown under

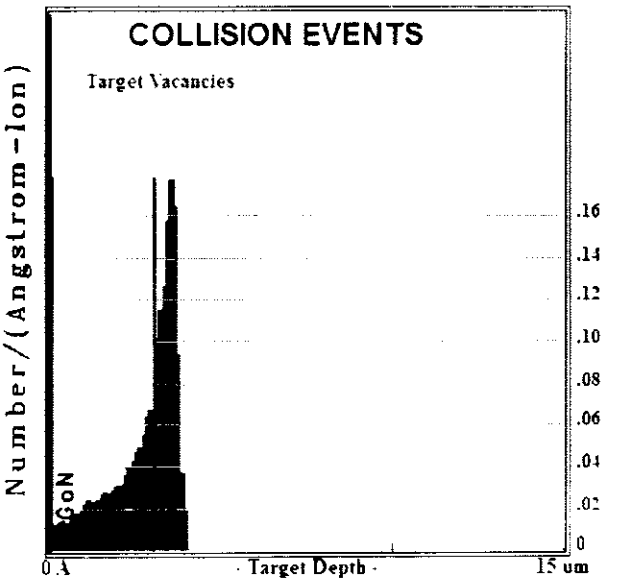

Fig 16: Collision events oxygen at 3.15MeV

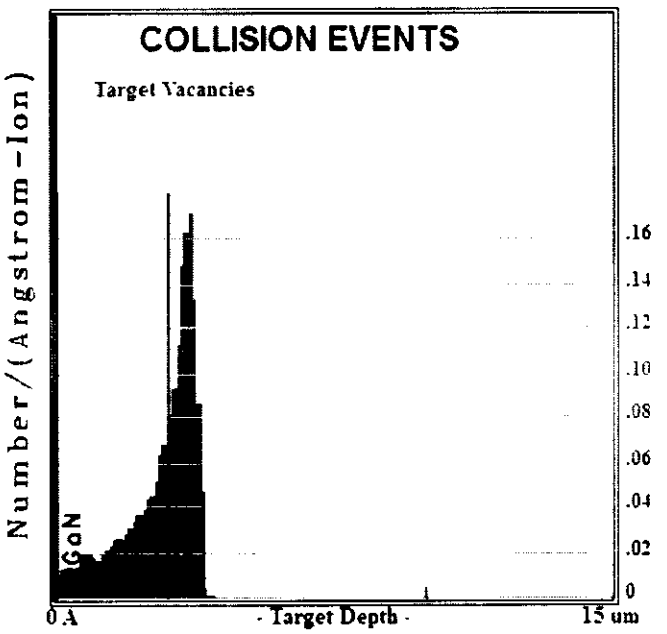

Fig 17: Collision events oxygen at 3.3MeV

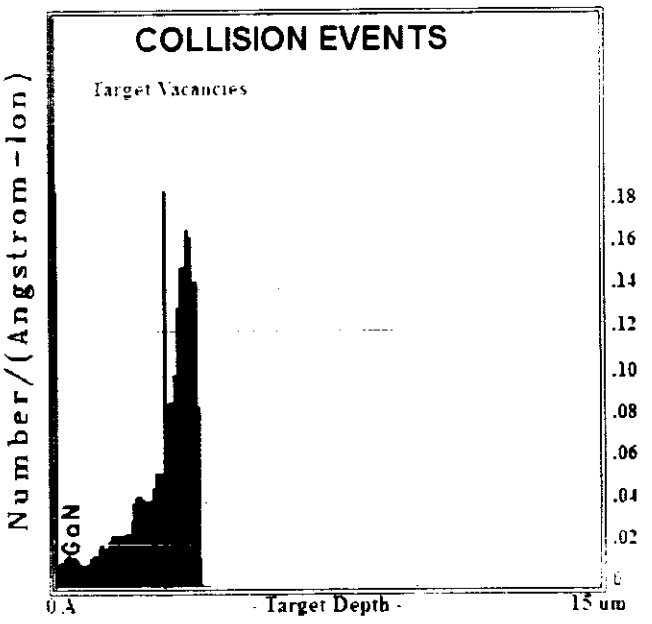

Fig 18: Collision events oxygen at 3.3MeV

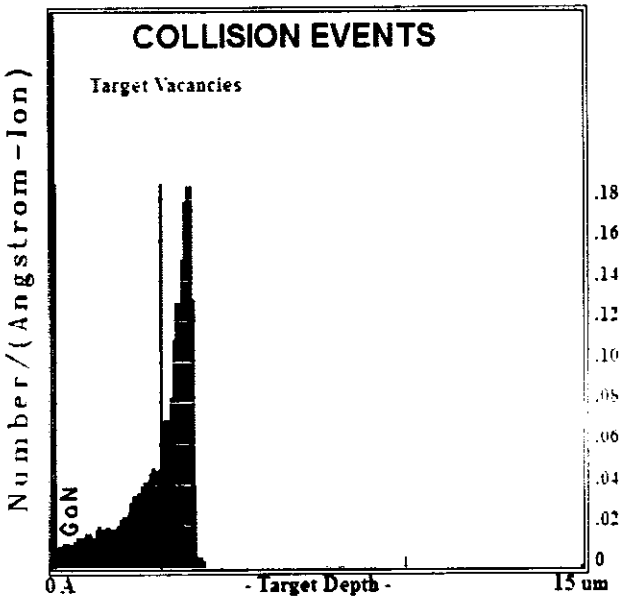

Fig 19: Collision events oxygen at 3.45MeV

To above mentioned plots (fig 4.10- 4.13) are generated by SRM 2008. Each data point is representing damage crated by specific energy. Damage created by Oxygen ion changes as the implanted energy is changed. For the ion energy of 3.15 MeV maximum damage created is 0.0185 vac/ion/ang and this damage is crated at depth of 36000 A in the structure.

Table 4: Table showing damage calculation w.r.t. depth attained by Oxygen ions

Ion Energy (MeV)	Ion Ranges Rp (um)	Extent of Damages (%) (vac/ion/ang)
3.15	3.52	0.0185x100=1.85
3.30	3.60	0.0180x100=1.80
3.45	3.66	0.0190x100=1.90
3.60	3.75	0.0187x100=1.87

For other high energies of 3.15 MeV, 3.45 MeV and 3.60 MeV damage crated is 0.0180 vac/ion//ang. And 0.0187 vac/ion/ang. Respectively.

4.2.4 Damage Calculation for Fluorine

Implanted energies used for fluorine are 3.40 MeV, 3.50 MeV, 3.65 MeV and 3.75 MeV. Now fluorine ions are implanted in the device structure shown above using these mentioned energies in simulation and a damage profile is obtained for each category, as shown under

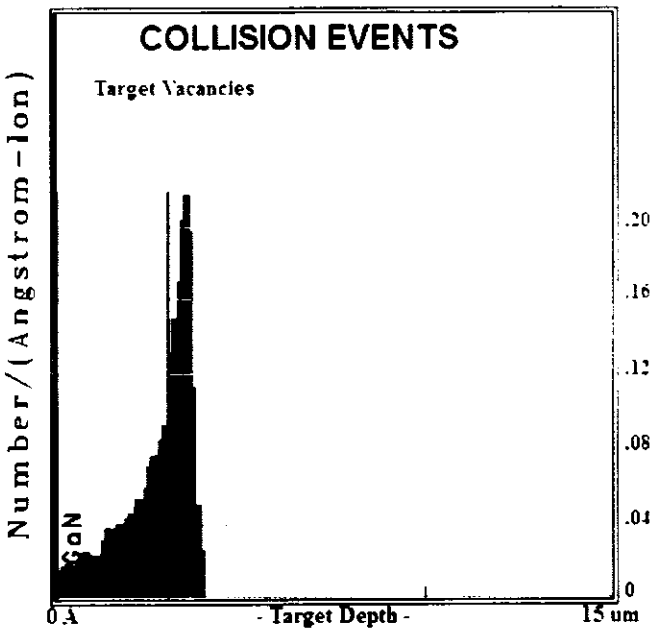

Fig 20: Collision events oxygen at 3.40MeV

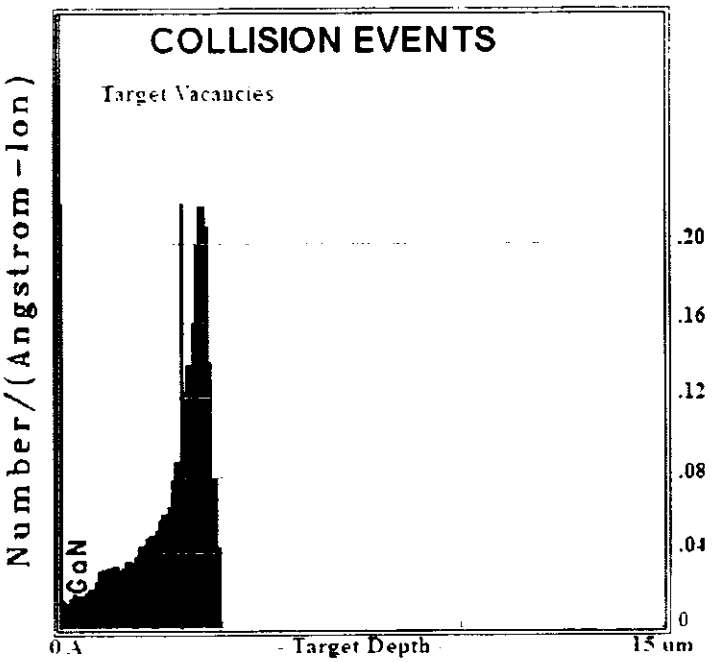

Fig 21: Collision events oxygen at 3.5MeV

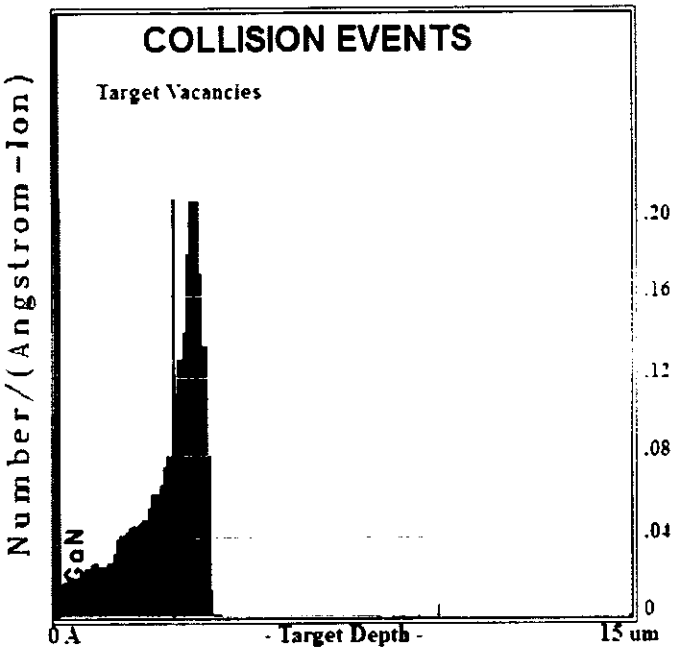

Fig 22: Collision events oxygen at 3.65MeV

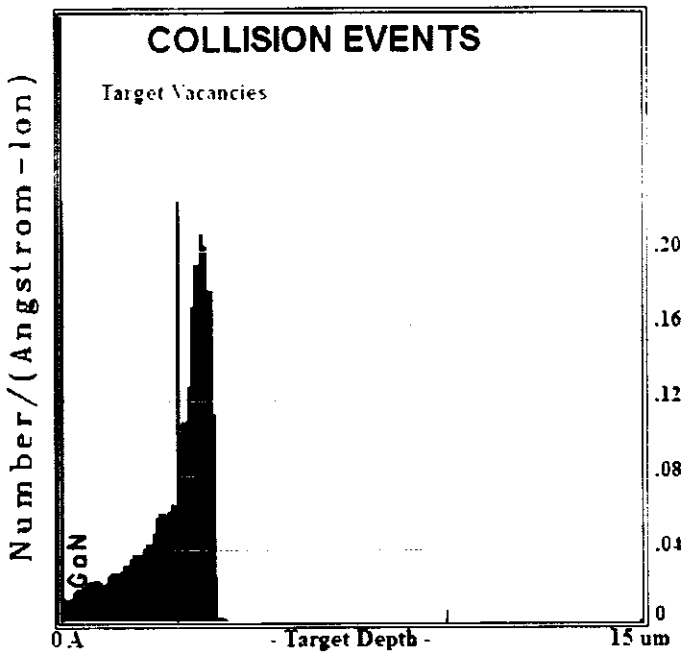

Fig 23: Collision events oxygen at 3.75MeV

The above mentioned plots (fig 4.14-4.17) are generated by SRIM 2008. Each data point is representing damage created by specific energy. Damage created by Fluorine ion changes as the implanted energy is changed. For the ion energy of 3.40 MeV maximum damage crated is 0021 vac/ion/ang and this damage is crated at depth of 34500 A in the structure.

Table 5: *Table showing damage calculation w.r.t. depth attained by Fluorine ions*

Ion Energy (MeV)	Ion Ranges Rp (um)	Extent of Damages (%) (vac/ion/ang)
3.40	3.52	0.021x100=2.10
3.50	3.57	0.019x100=1.90
3.65	3.64	0.020x100=2.0
3.75	3.72	0.021x100=2.1

For other high energies of 3.50MeV, 3.65MeV and 3.75MeV damage rated is 0.019 vac/ion/ang., 0.20 vac/ion/ang. And 01.021 vac/ion/ang., respectively.

4.2.5 Damage Calculation for Chlorine

Implanted energies used for Chlorine are 4.65 MeV, 4.95 MeV, 5.15 MeV and 5.30 MeV. Now Chlorine ions are implanted in the device structure shown above using these mentioned energies in simulation and a damage profile is obtained from each category, as shown under

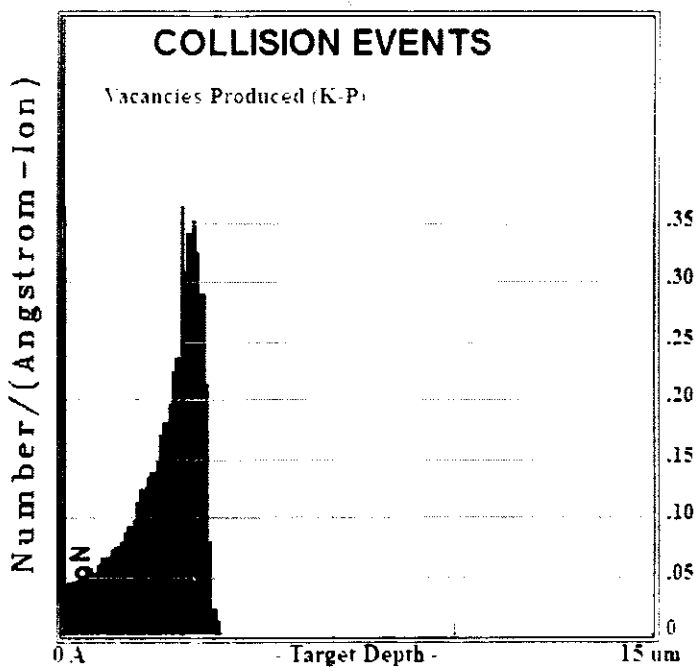

Fig 24: Collision events Chlorine at 4.65MeV

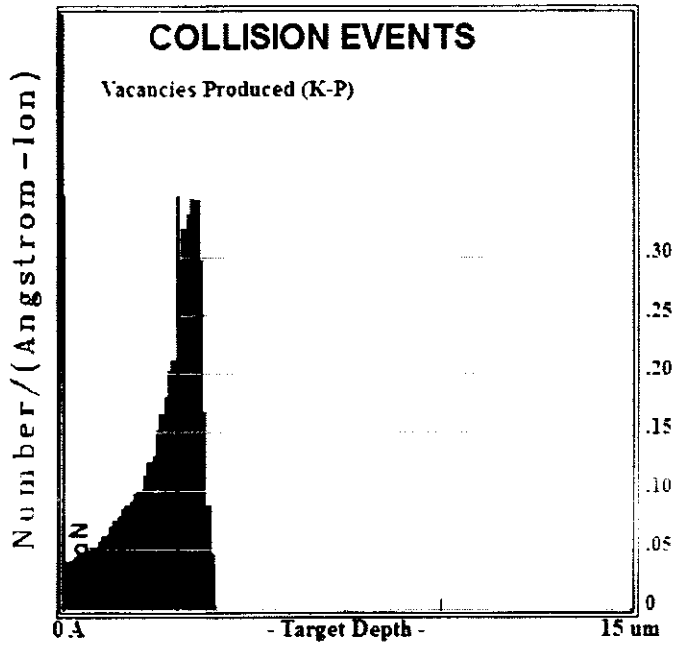

Fig 25: Collision events Chlorine at 4.95MeV

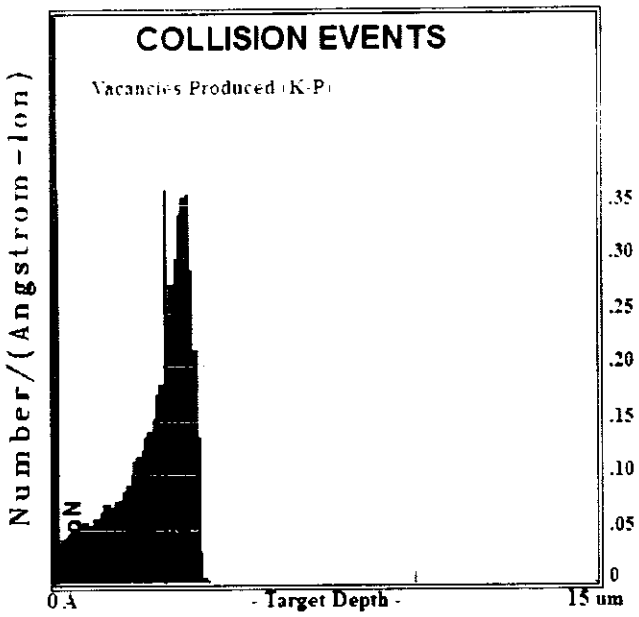

Fig 26: Collision events Chlorine at 5.15MeV

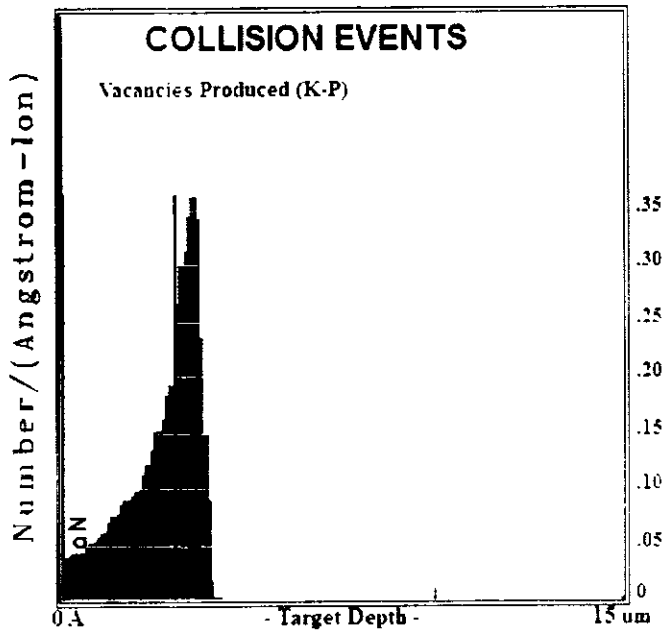

Fig 27: Collision events Chlorine at 5.3MeV

The above mentioned plots (fig 4.18-4.21) are generated by SRIM 2008. Each data point is representing damage crated by specific energy. Damage created by Chlorine ion changes as the implanted energy is changed. For the ion energy of 4.65 MeV maximum damage created is 0.0260 vac/ion/ang and this damage is created at depth of 34500 A in the structure.

Table 6: *Table showing damage calculation w.r.t. depth attained by Chlorine ions*

Ion Energy (MeV)	Ion Ranges Rp (um)	Extent of Damages (%) (vac/ion/ang)
4.65	3.36	0.0260x100=2.60
4.95	3.46	0.0264x100=2.64
5.15	3.55	0.0270x100=2.70
5.30	3.58	0.0265x100=2.65

For other high energies of 4.95MeV, 5.15 MeV and 5.30 MeV damage crated is 0.0264 vac/ion/ang., 0.0270 vac/ion/ang. And 0.0265 vac/ion/ang. Respectively.

4.2.6 Damage Calculation for zinc

Implanted energies used for Zinc are 6.90 MeV, 7.10 MeV, 7.30 MeV and 7.40 MeV. Now Zinc ions are implanted in the device structure shown above using these mentioned energies in simulation and a damage profile is obtained for each category, as shown under

The above mentioned plots (fig 4.26-4.29) are generated by SRIM 2008. Each data point is

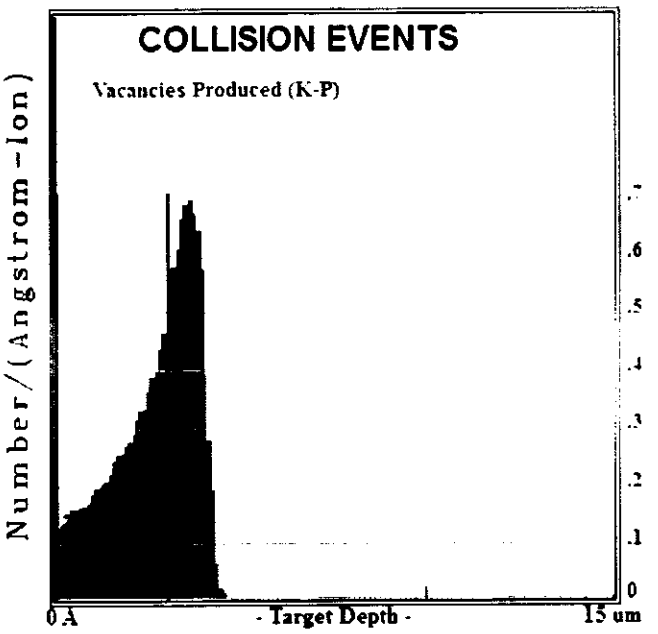

Fig 28: Collision events Chlorine at 6.9MeV

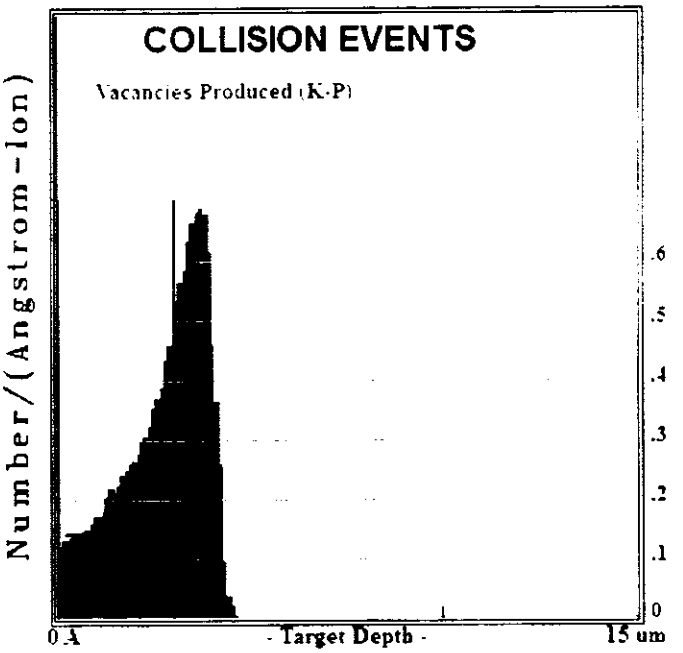

Fig 29: Collision events Chlorine at 7.1MeV

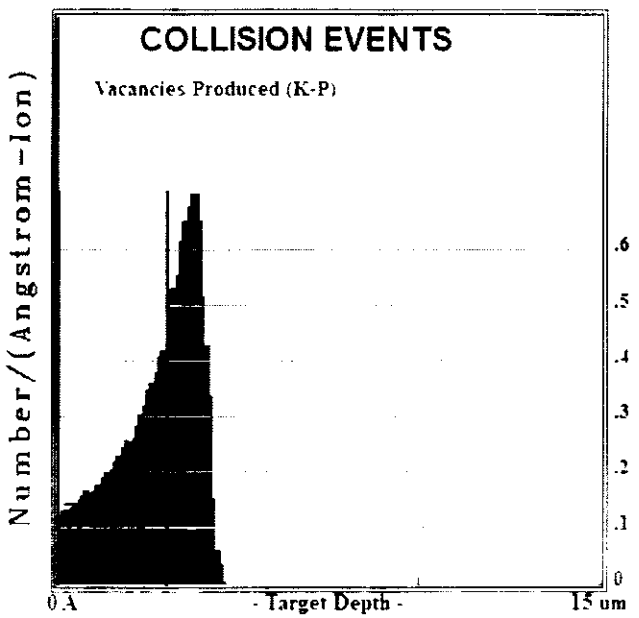

Fig 30: Collision events Chlorine at 7.3MeV

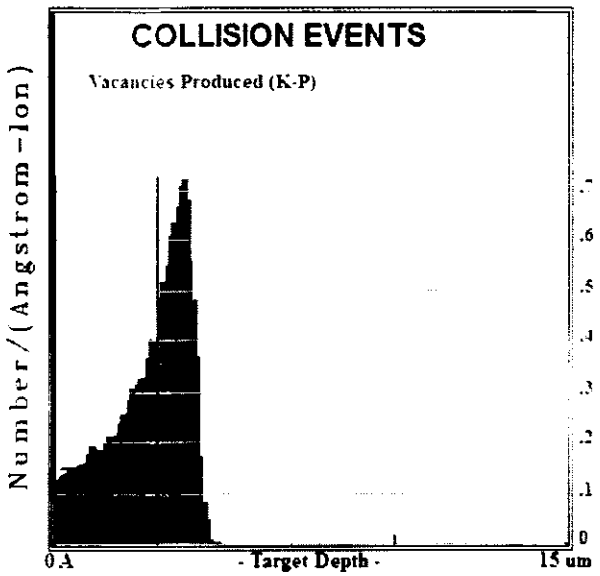

Fig 31: Collision events Chlorine at 7.4MeV

Representing damage created by specific energy. Damage created by Zinc ion changes as the implanted energy is changed. For the ion energy of 6.90 MeV maximum damage created is 0.0359 vac/ion/ang and this damage is created at depth of 37500 A in the structure

Table 7: *Table showing damage calculation w.r.t. depth attained by Zinc ions*

Ion Energy (MeV)	Ion Ranges Rp (um)	Extent of Damages (%) (vac/ion/ang)
6.90	3.68	0.0359x100=3.59
7.10	3.80	0.0363x100=3.63
7.30	3.82	0.0352x100=3.52
7.40	3.86	0.0353x100=3.53

For other high energies of 7.10 MeV. 7.30 MeV and 7.40 MeV damage crated is 0.0363 vac/ion/ang.. 0.0352 vac/ion/ang. And 0.0353 vac/ion/ang. Respectively.

4.3 Damage calculation of Silicon

Various experiments were performed with silicon, as silicon has some special properties; it can act as donor and acceptor, plus the ease with which we can manipulate its properties to our advantage makes it a good choice. Silicon atom was bombarded on our structure at varying energy levels and different results were achieved

Table 8: Table showing damage calculation w.r.t. depth attained by Silicon ions

s.no	Energy KeV	Range (A)	%Damage=(vac/ion/avg range) *100
1	125	1574.9	70.29
2	250	3067.6	54.09
3	375	4555.7	44.75
4	500	5926.2	39.05
5	625	7151	35.25
6	750	8282.7	32.41
7	875	9290.8	30.30
8	1000	10250	28.46

This table shows different trends, to further explore these trends different curves were drawn using the Mat lab; these are energy vs. damage and energy vs. range curve.

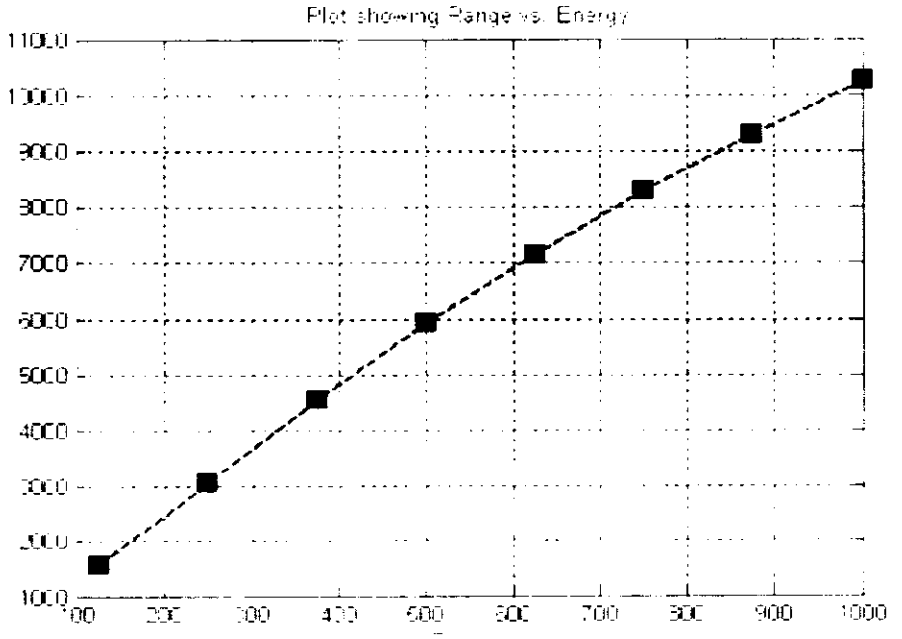

Fig 32:Range vs Energy plot for Silicon ion

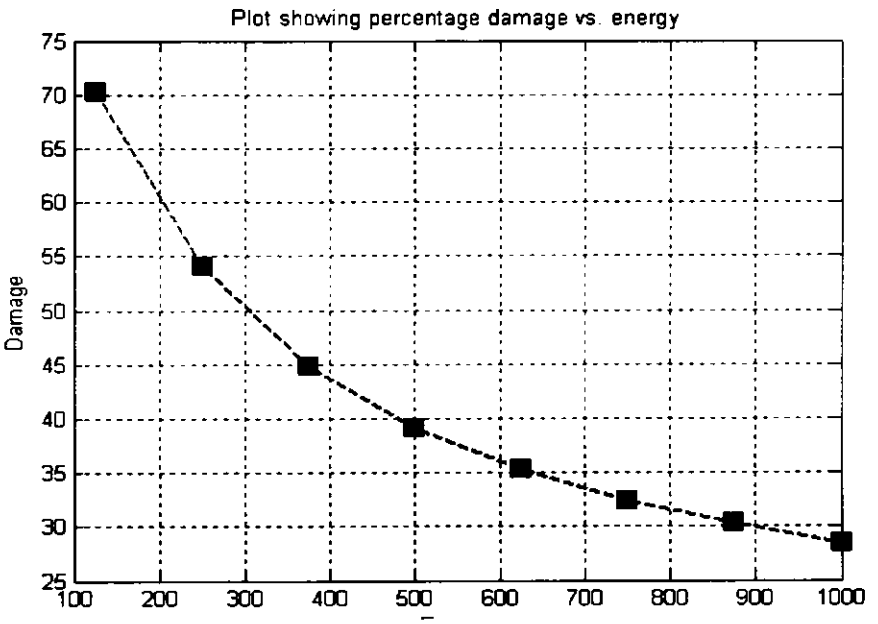

Fig 33:Energy vs %Damage plot for Silicon ion

As it is obvious that this energy vs. range curve shows a sort of proportional relationship while the energy vs. %damage curve shows a sort of an indirect relationship, this means that greater the energy greater will be the penetration of the ion in to the structure which is quite an obvious concept, but the interesting part is that at higher energies the percentage damage reduces, that is at higher energies the damage that an ion produces reduces significantly, moreover this fall in percentage damage is not uniform but it is sharper at lower energies and less sharp at higher energies, so what we get from this plot is that not only the higher energy levels are difficult to attain physically but they are also less productive when it comes to damage production. This lead us performing some experiments at lower energies, experiments were performed at energies lower than 100KeV and following results were obtained.

Table 9: *Table showing damage calculation w.r.t. depth attained by Silicon ions at lower energies*

s.no	Energy KeV	Range(A)	%Damage=(vac/ion/range)*100
1	10	165.09	99.06
2	15	230.05	100
3	20	294.75	99.175
4	25	358.6	97.59
5	30	421.28	96.01
6	35	484.96	93.90
7	40	543.03	92.95
8	45	608.99	90.46

Again these results were plotted in order to analyze the trends arising from this data

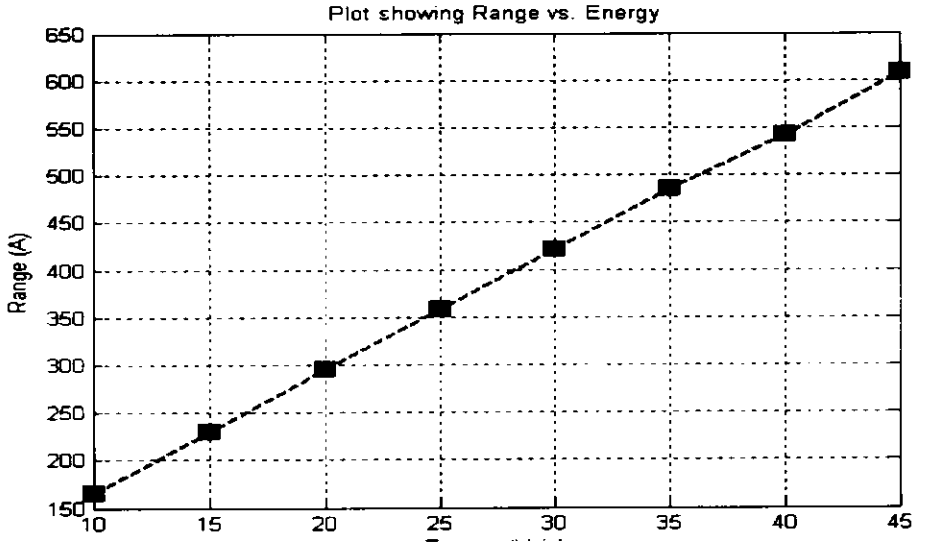

Fig 34:Range vs Energy plot for Silicon ion at lower energies

While the range for this data is not as great as was for the earlier data, the percentage damage column shows a major improvement, it is quite interesting to note that the percentage damage touches 100% at 15KeV and shows a downwards trend afterwards, this further emphasises our earlier point that at lower energies

the percentage damage is higher while the range is lower and we can sy this reason able authority that 15 KeV is the optimum point where the percentage damage is maximum.

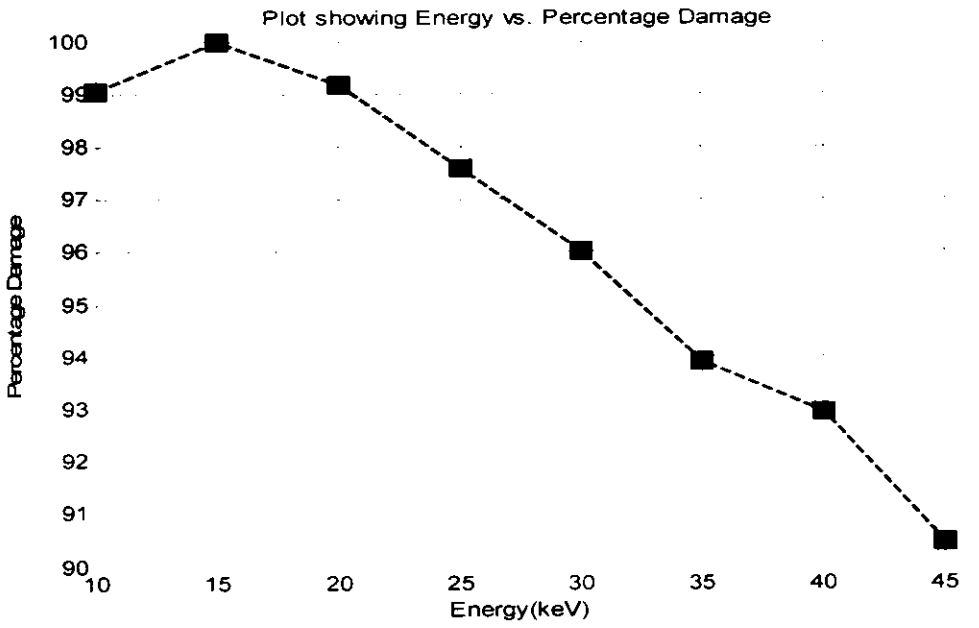

Fig 35:Energy vs %Damage plot for Silicon ion at lower energies

4.4: Bombardment of some other ion species

In order to check the merits and demerits, some other ion species were also bombarded on the target structure, the important features to decide were the energy required to push the ions with reasonable force, and to draw a comparative analysis, among each other. After a lot of experimentation, it was found out that many ions are too heavy and the energy required to accelerate them and create a considerable damage is too high, and it is almost physically impossible to generate that much energy, on the other hand the respective percentage damage is to low and not acceptable, these reason also contributed to the selection of silicon as the choice atom to bombard on the target structure. Following table shows some of the results of the experiments performed using other atoms.

Table 10: Table showing damage calculation w.r.t. depth attained by other ion specie

No	Bombarded ion	Energy(MeV)	Range(A)	%Damage
1	Boron	4	44444	1.82
2	Carbon	4	37768	2.67
3	Oxygen	4	31766	5.18
4	Neon	4	30209	8.26

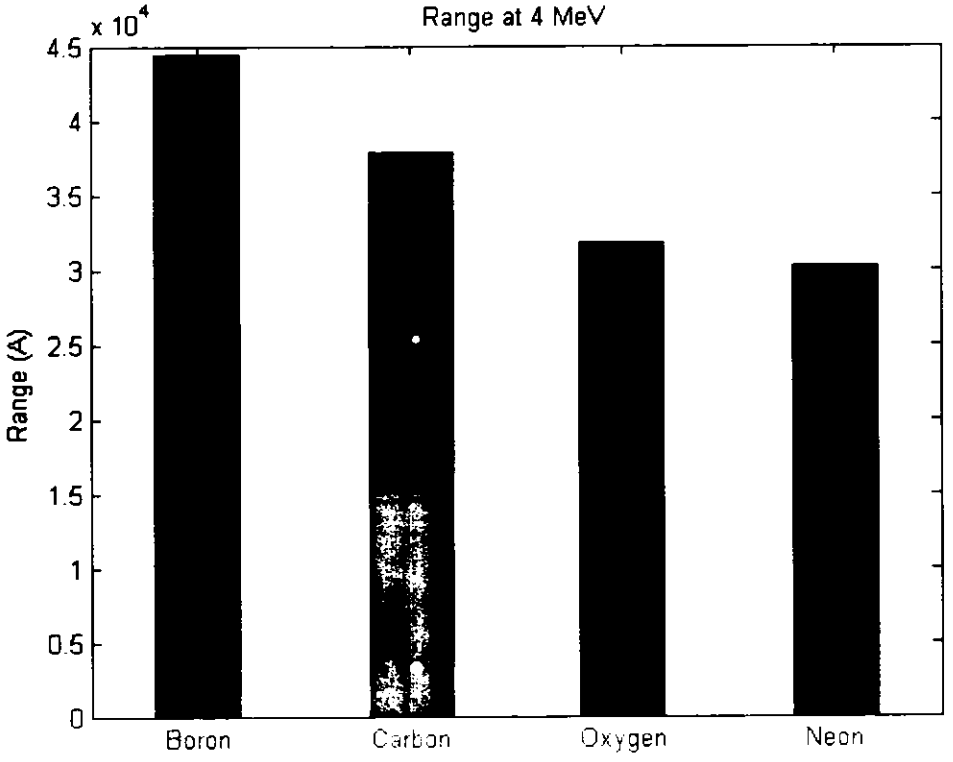

Fig36: Ranges for other ions at 4MeV

4.5: Bombardment of Silicon on individual layers

After all the experimentation it was felt that the bombardment of silicon on individual layers is a better idea, as it gives as layer by layer analysis of the target structure, keeping this in view silicon at different energy was bombarded at different layers of the target device and following results were obtained.

Table 11: *Table showing damage calculation w.r.t. depth attained by Silicon ions on SiC*

Sr.no	Energy(KeV)	Range(A)	%damage
1	150	1880.4	65.74
2	175	2173.7	62.25
3	200	2478.9	58.97
4	225	2779.4	56.18

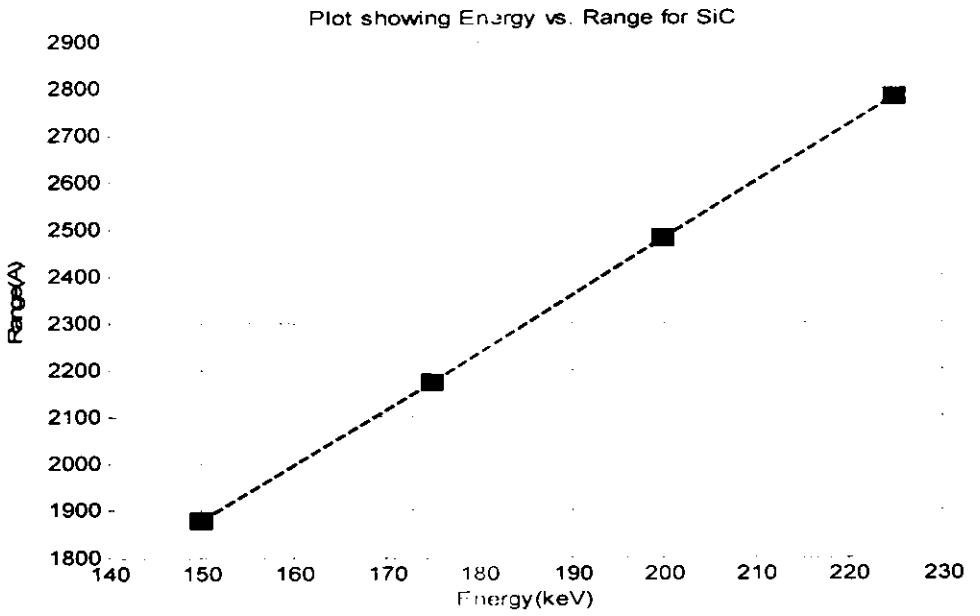

Fig 37: Energy vs Range Plot for SiC layer

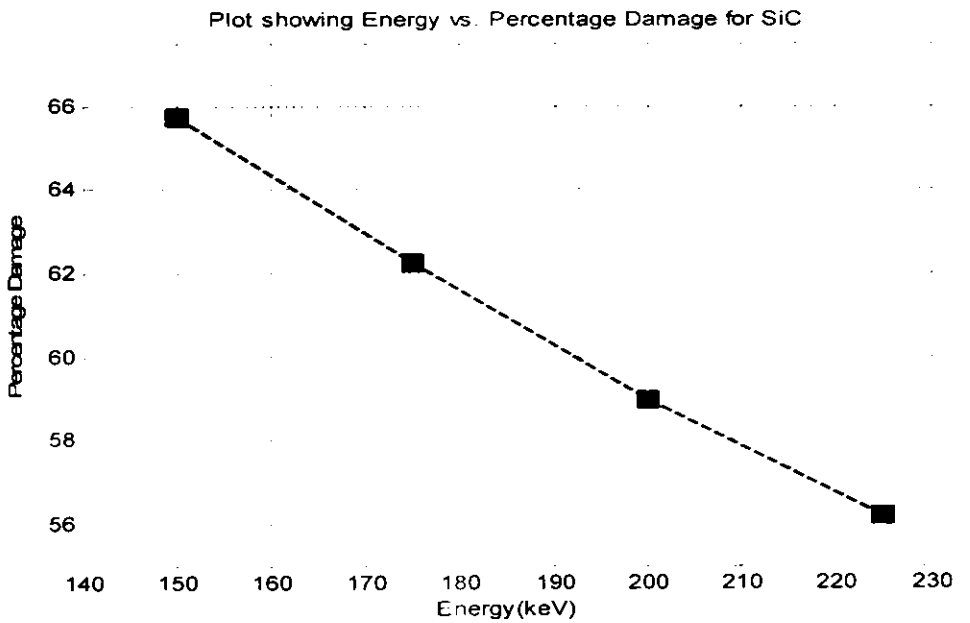

Fig 38:Energy vs percentage damage Plot for SiC layer

SiC is the substrate layer 380um thick and silicon atom were bombarded at it at some energy, the reults again proves our previous hypothosis, first of all at higher energies the range becomes higher and the percentage damage becomes lower secondly the figures in both the columns of percentage damage and energy are in acceptable limits, which testifies for the suitability of the silicon atom to be used as the choice atom to be bombarded on the target structure. A target damage with in the range of fifties and sixties percent was achieved, which is quite a reasonable figure.

GaN

Table.12: *Table showing damage calculation w.r.t. depth attained by Silicon ions on GaN*

Sr.no	Energy(KeV)	Range(A)	%damage
1	150	2052.1	65
2	175	2399.4	62.09
3	200	2753.1	59.34
4	225	3112.6	56.81

Same level of energies were used to bombard the GaN layer, 3um thick, the above mentioned table shows the result. Again the percentage damage column shows round about the same figures howering between 55 and 65 percent, the highest of them being 65 percent. the ranges in case of GaN is higher than the ranges for SiC. This might be due to some intrinsic property of Galium nitride, like strength of the bond, bond length etc. Now let us see how alimunium galium nitride reacted to the bombardment of silicon atom at same energies. The graphs below show the energy vs range in angstrom and energy vs percentage damage curves.

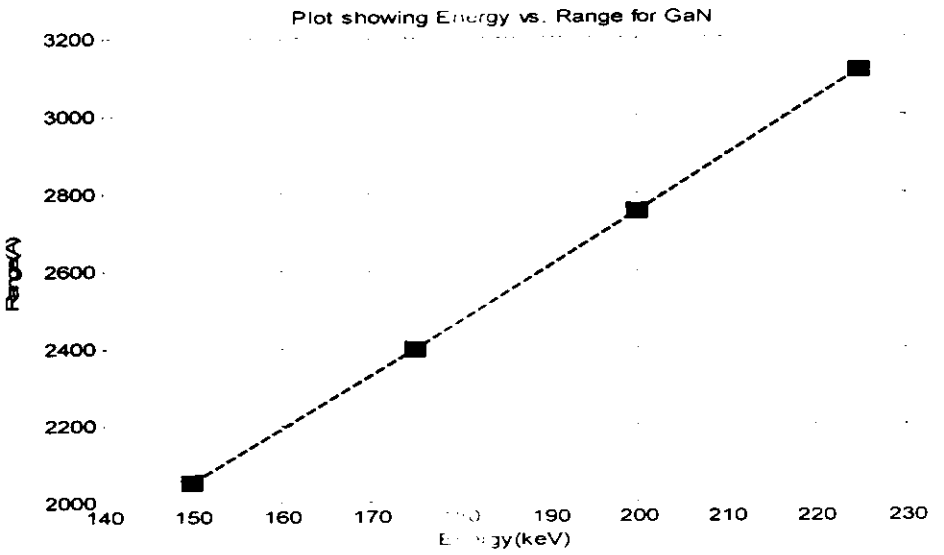

Fig 39:Energy vs Range Plot for GaN layer

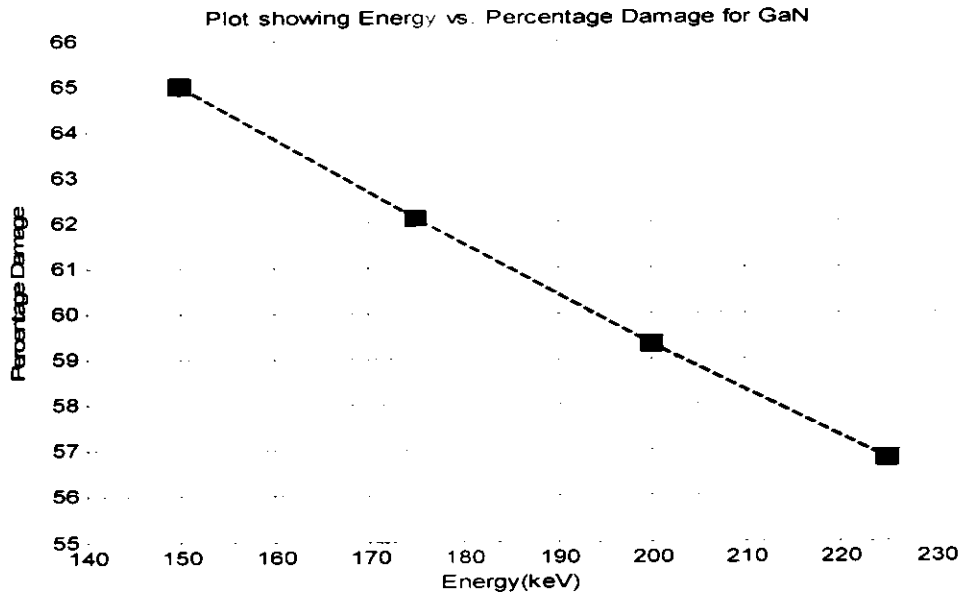

Fig 40:Energy vs percentage damage Plot for GaN layer

Now let us explore how AlGaN 20nm thick layer reacted to the bombardment of silicon atom at same energy. The following table gives an insight.

AlGaN

Table 13: *Table showing damage calculation w.r.t. depth attained by Silicon ions on AlGaN*

Sr.no	Energy(KeV)	Range(A)	%damage
1	150	128.29	38.88
2	175	141.22	31.89
3	200	94.076	44.37
4	225	92.058	42.10

The above table shows that the percentage damage was maximum in the case when energy was 200KeV, and no valid result was produced at energy level of 225 KeV. The percentage damage was also maximum at 200KeV. The following graphs further elaborates the table.

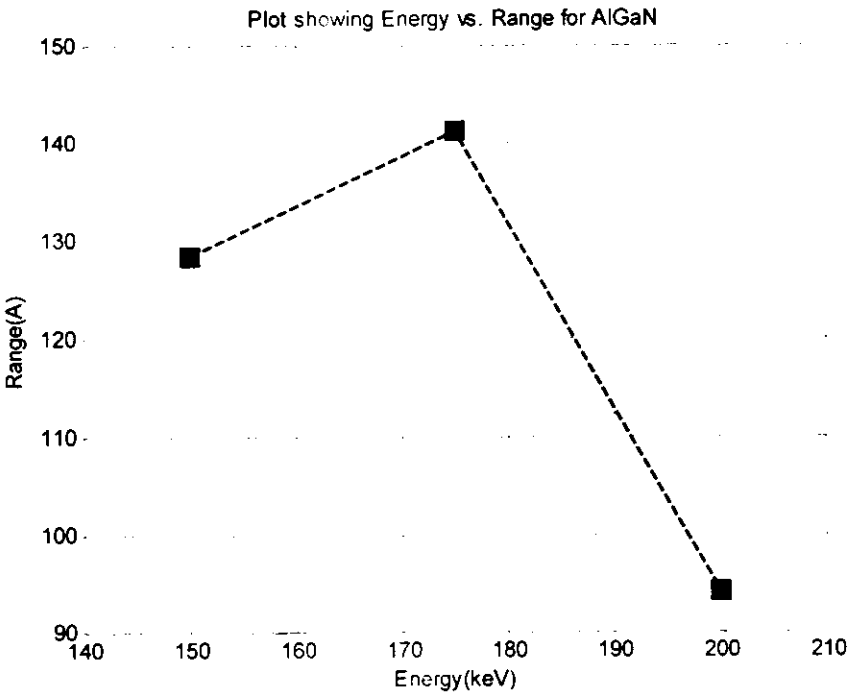

Fig 41:Energy vs Range Plot for AlGaN layer

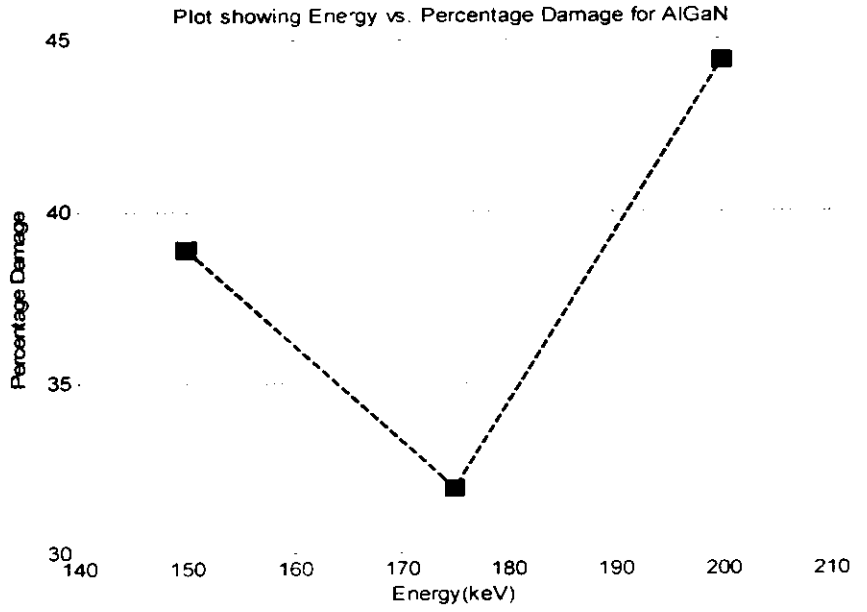

Fig 42:Energy vs percentage damage Plot for AlGaN layer

The fourth layer of Galium nitride is orignally just 3nm thick, this is too thin to get a result from, so it was decided to increase it's thickness to 30nm in order to get the data from experimentation. The following results were achieved after experimentation.

GaN1

Table 14: *Table showing damage calculation w.r.t. depth attained by Silicon ions on GaN1*

s.no	Energy(KeV)	Range(A)	%damage
1	150	139.54	58.46
2	175	153.29	49.51
3	200	239.23	29.22
4	225	127.39	50.21

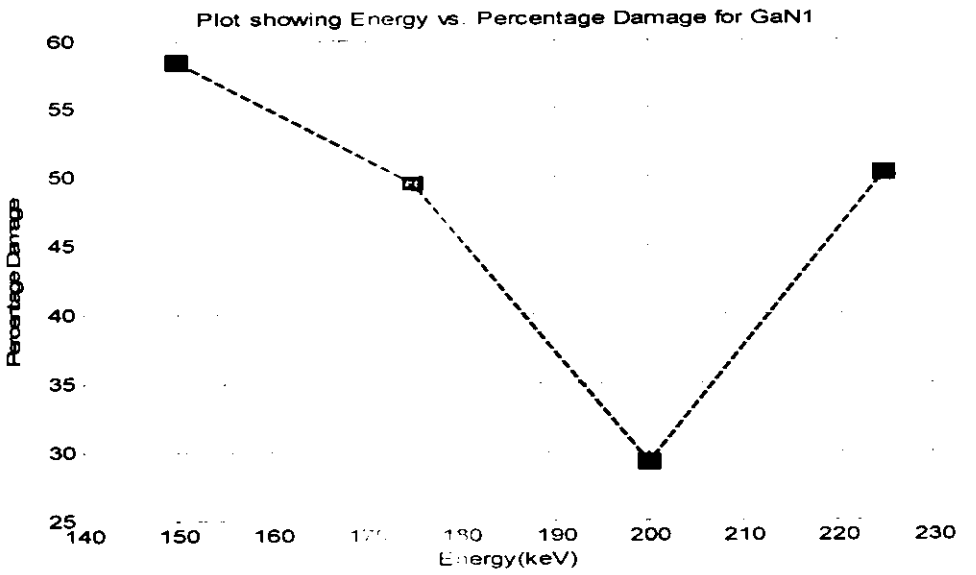

Fig 43:Energy vs percentage damage Plot for GaN layer

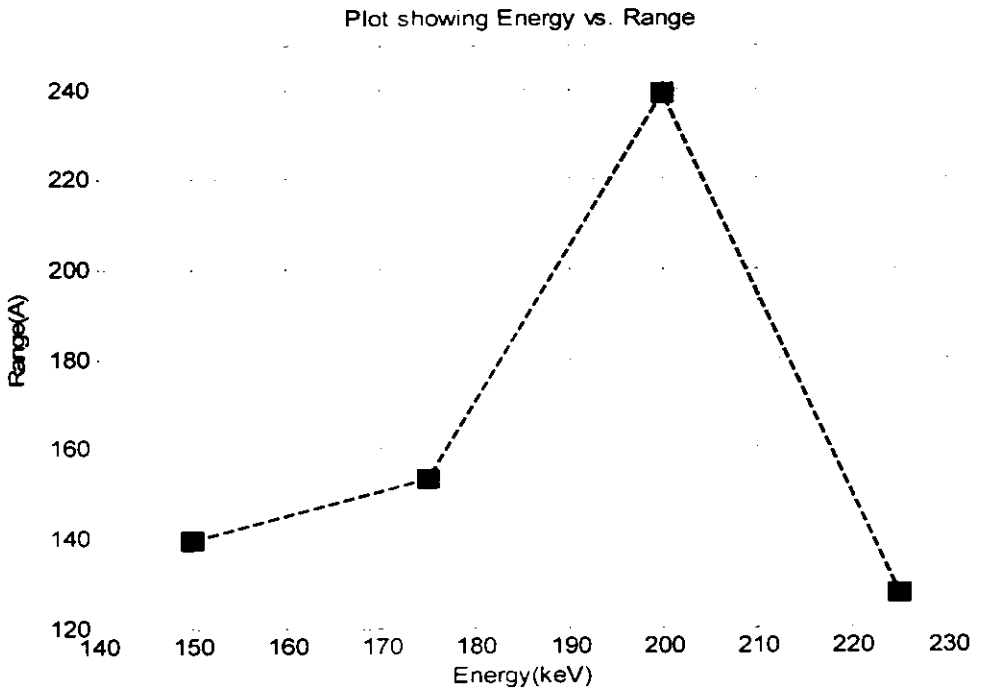

Fig 44:Energy vs Range Plot for GaN layer

The thing worth mentioning here is the steep fall in the percentage damage at 200KeV, and what makes it even more interesting that there is a jump in range column at the same point

4.6 Some lower energies

As mentioned earlier at lower energies the results in terms of percentage damage is better, therefore it is a good idea to repeat these experiments at lower level, again first of all the substrate layer of silicon carbide was bombarded with the silicon atom at different energies ranging from 50KeV to 125KeV and following results were obtained.

Table 15: *Table showing damage calculation w.r.t. depth attained by Silicon ions on SiC*

s.no	Energy(KeV)	Range(Å)	%damage
1	50	673.52	88.36
2	75	978.73	80.92
3	100	1277.8	75.10
4	125	1574.9	70.29

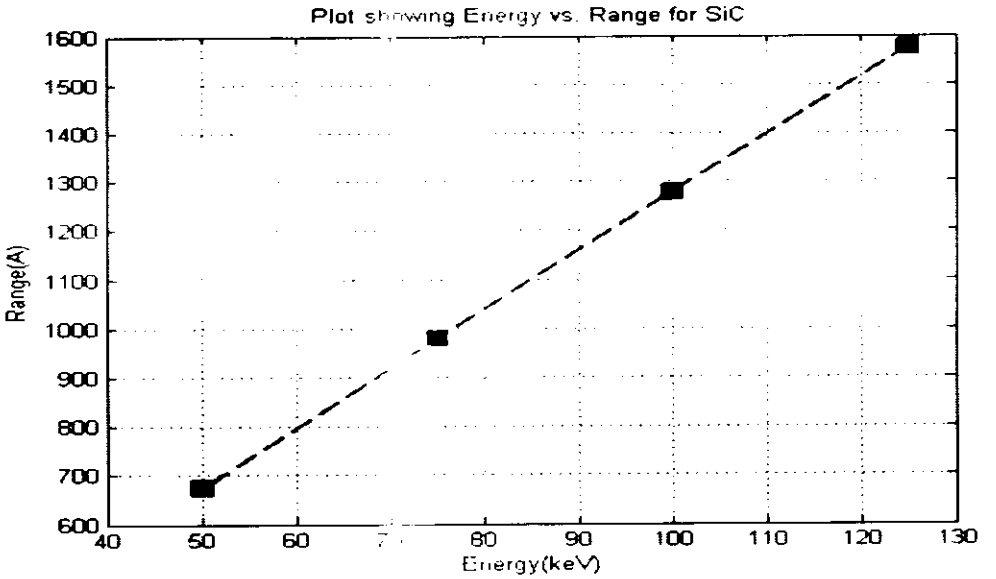

Fig 45:Energy vs Range Plot for SiC layer at lower energy

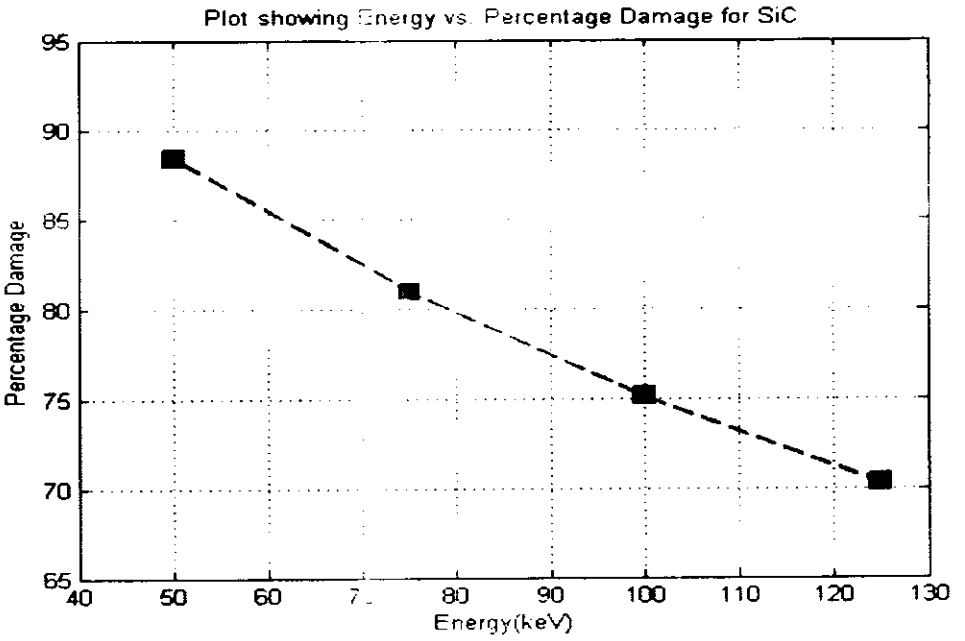

Fig 46:Energy vs Percentage Damage Plot for SiC layer at lower energy

At lower level energy levels the range is lower but the percentage damage is higher. Then the second 3 um thick layer of GaN was choosed for the bombardment of silicon atom, and following results were obtained.

Table.16: *Table showing damage calculation w.r.t. depth attained by Silicon ions on GaN (lower energies*

s.no	Energy(KeV)	Range(A)	%damage
1	50	703.45	80.43
2	75	1033	76.34
3	100	1368	71.99
4	125	1706.7	68.39

)

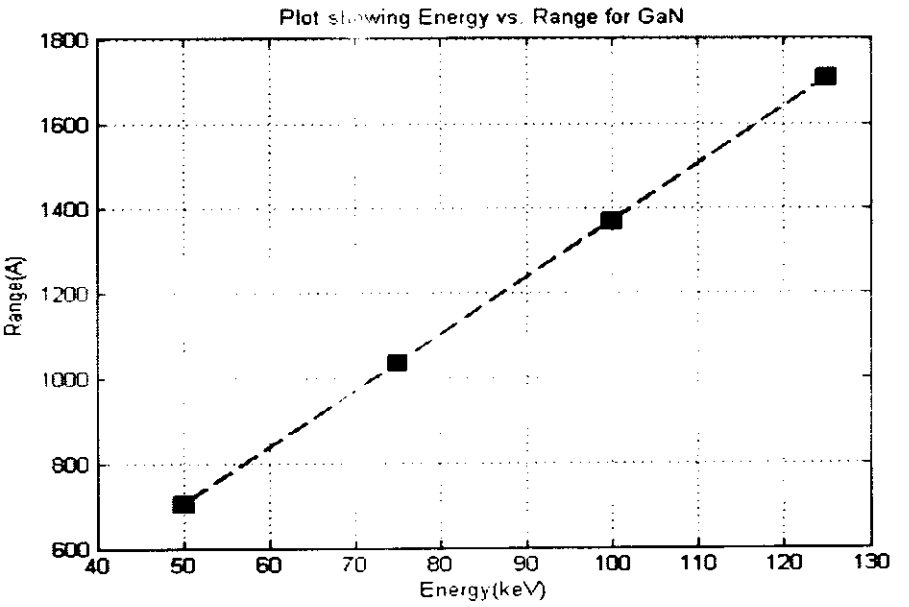

Fig 47:Energy vs Range Plot for GaN layer at lower energy

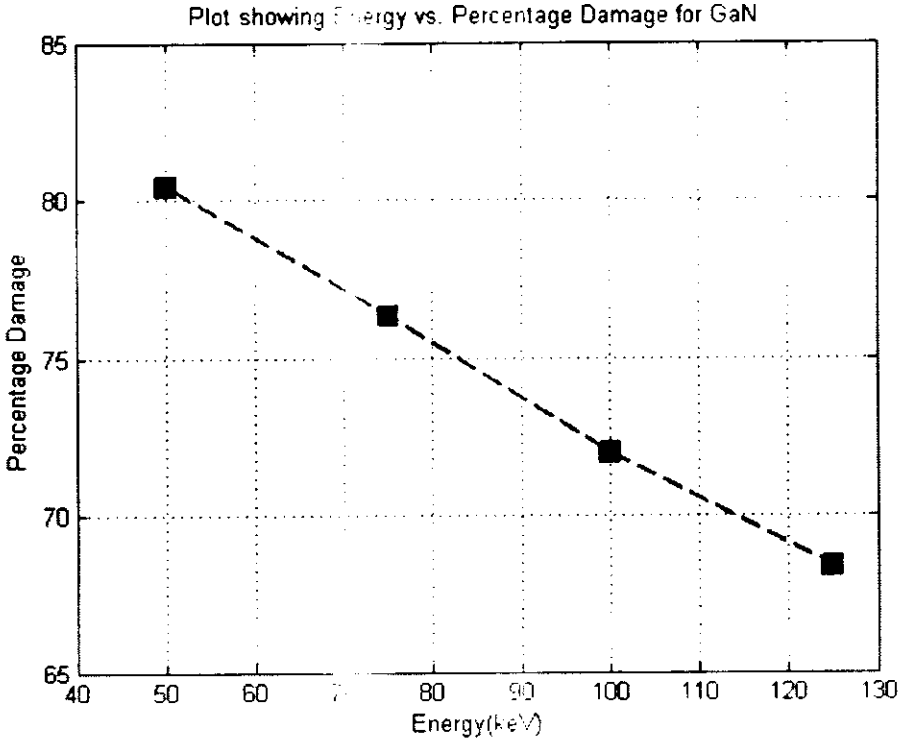

Fig 48:Energy vs Percentage Damage Plot for GaN layer at lower energy

Again you see higher level of percentage damage as compared to the previous graph at lower energy level. Next the 20nm Aluminum Gallium nitride was bombarded with the silicon atom and following results were obtained.

Table 17: *Table showing damage calculation w.r.t. depth attained by Silicon ions on AlGaN (lower energies*

s.no	Energy(KeV)	Range(A)	%damage
1	50	100.14	92.14
2	75	106.4	67.72
3	100	111.67	55.55
4	125	95.171	56.74

)

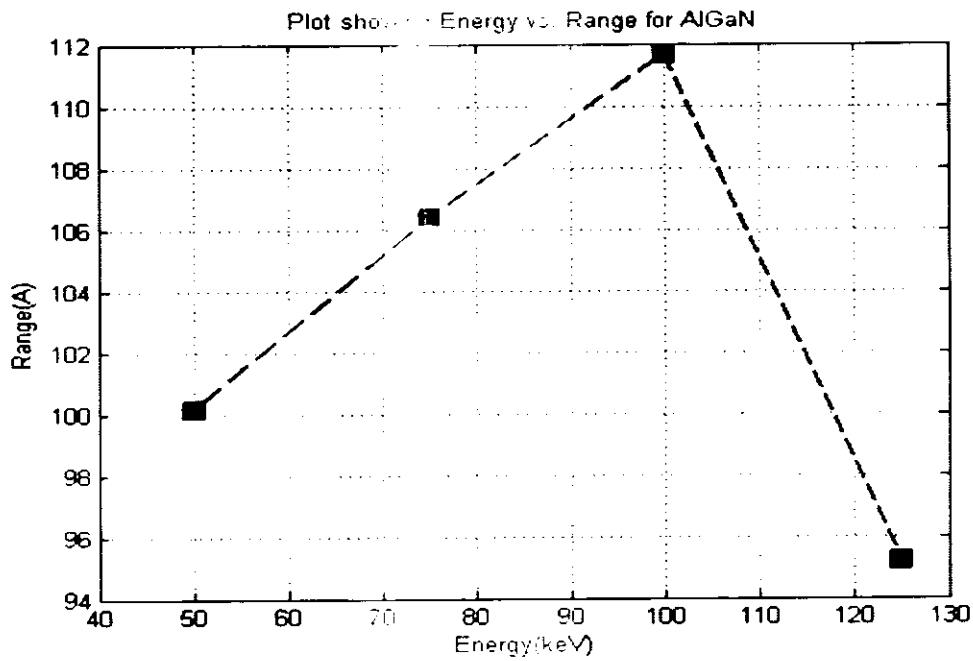

Fig 49:Energy vs Range Plot for AlGaN layer at lower energy

Here a peak was achieved in terms of the range at 100KeV but after that there is a sharp fall, so you can say that 100KeV is the maximum point in terms of range.

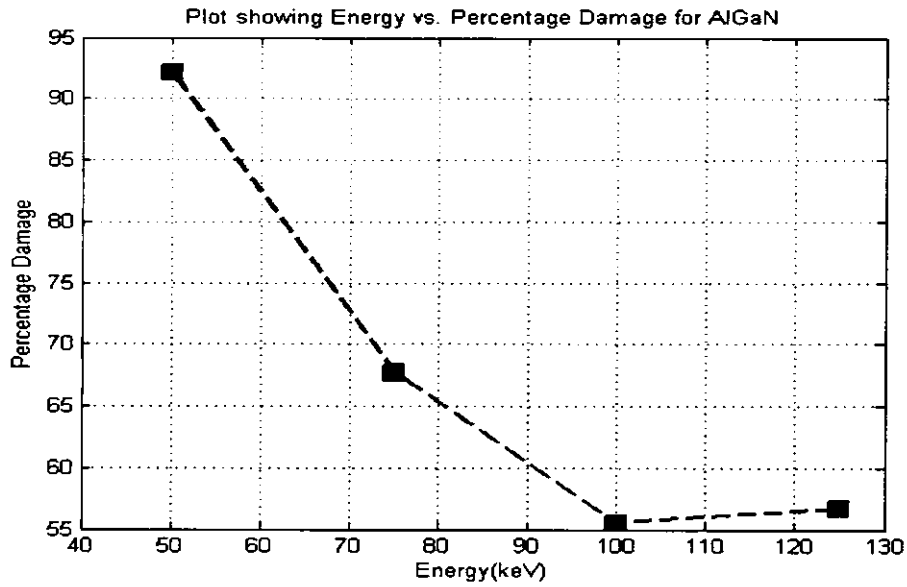

Fig 50: Energy vs Percentage Damage Plot for AlGaN layer at lower energy

Here we see an inverse trend as compared to the range graph; here 100 KeV is the minimum point in terms of the percentage damage. Now let's discuss the bombardment of the upper most layer of Gallium nitride that was thickened to a dimension of 30nm in order to get results from the experiment, following results were achieved.

Table 18: *Table showing damage calculation w.r.t. depth attained by Silicon ions on GaN1 (lower energies)*

s.no	Energy(KeV)	Range(A)	%damage
1	50	158.04	94.71
2	75	148.14	82.5
3	100	154.25	66.39
4	125	138.83	64.74

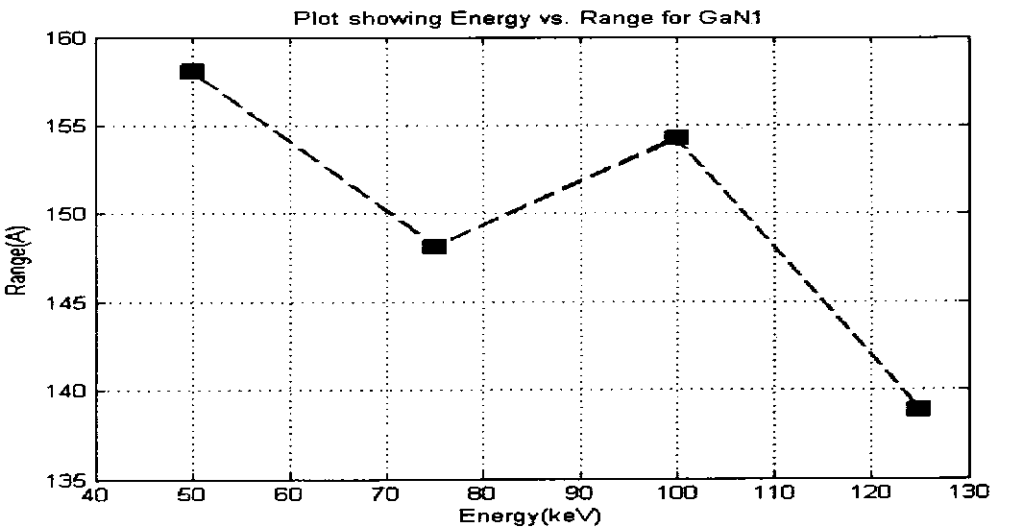

Fig 51:Energy vs Range Plot for GaN1 layer at lower energy

Generally there is a downwards trend as far as range is concerned except for a jump on the higher side in the middle of this graph.

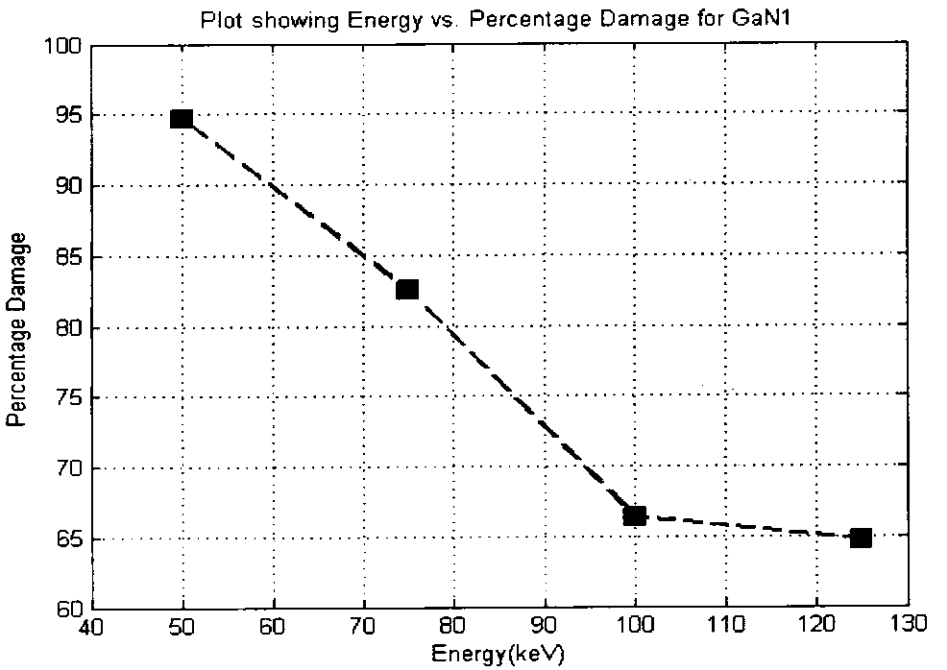

Fig 52:Energy vs Percentage Damage Plot for GaN1 layer at lower energy

Here the trend is similar to the projected outcome that is at lower energies percentage damage is higher and at higher energies it is relatively lower.

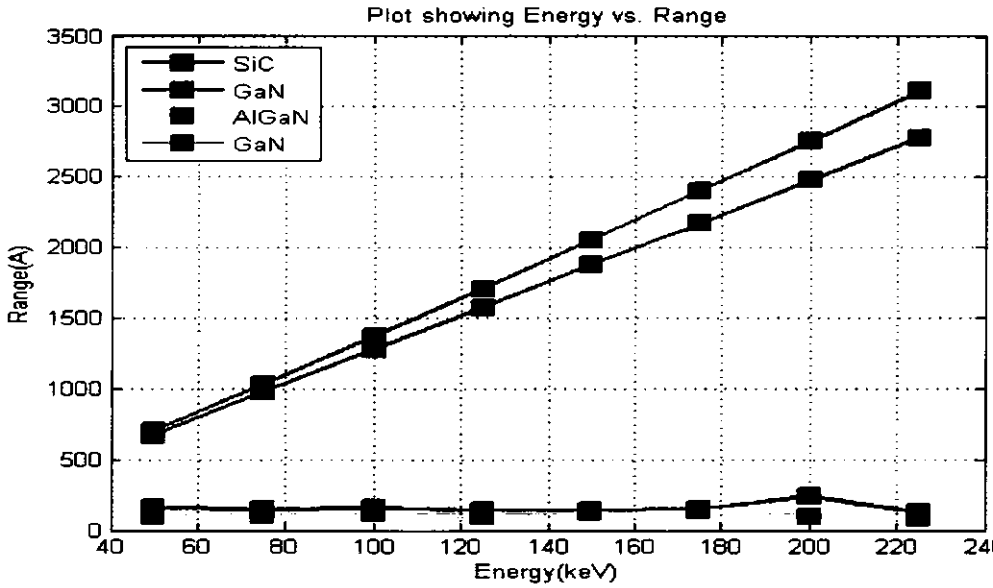

Fig 53: Cumulative Energy vs. Range

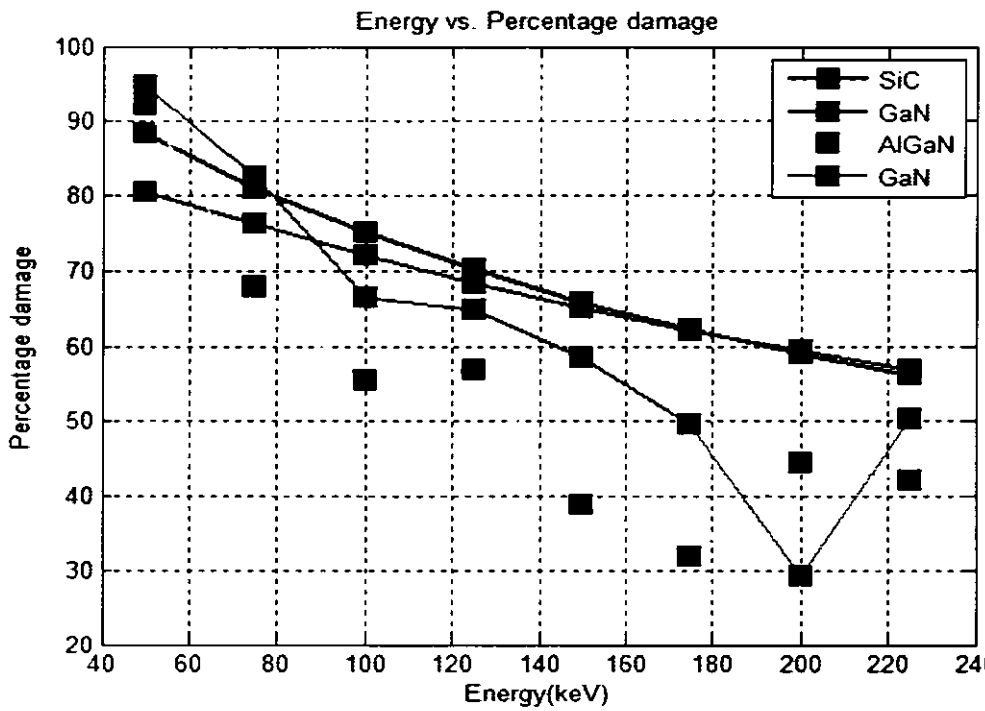

Fig 54: Cumulative Energy vs. Percentage Damage

4.7 Physical Basis of Our Model

The basic process for our work is as follows: damage is caused to the layer by implanting energetic ions into semiconductor crystal. Species are chosen so that they do not dope and create sufficient and uniform damage in the semiconductor. The depth of the damage can be varied by changing the ion energies. The implantation is usually performed at 7 to the substrate surface normal to prevent the channeling. We have used the similar angle of implantation in order to simulate the device structure. The ion impact caused vacancies and other defects to be formed. We have used the Kinchin-Pease model (KP Model) accounts for the defect generation, damage accumulation as well as the interstitial encountering. With two parameters, one species independent and other species – dependent, very good agreement with experimental impurities profile has been obtained. In addition, this model is believed to provide reasonable good profile for the interstitial profile [30]. Following are the assumption that we take into account for our suggested simulated process scheme:

a) First of all, defect production is taken into account by calculating the deposited energy E for each cascade by using the binary collision approximation.

b) This energy is then converted into the number of point defect n by using the Kinchin-Pease formula [31]

$$N = kE/2Ed \qquad (4.1)$$

Where k=0.8 is a constant, and Ed is the displacement threshold energy (15eV) for Ga based materials.

c) Damage accumulation is then calculated as all of the defects are calculated by Eq. (4.1) can not survive, since some of the defects might recombine with in the cascade as well as with the defect generated by previous cascade.

d) The crystal is then annealed; the vacancies formed are suggested to be highly mobile.

4.8 Comparison of the Six Ion Specie

It is well known that the nature of implantation defects created by light and heavy ions are quite different [23, 24, and 25]. For light ion like He, most of the residual defects after implantation are in form of point defects and dilute defect clusters, whereas for heavy ions like Zn and Cl in addition to point defect, other defects such as denser defect clusters, complexes and extended defects are expected to be found [28].

Helium is highly mobile inside the lattice and produces sufficient damage. Helium is not chemically active at higher annealing temperatures and does not affect the electrical properties of the device because of the inert nature of helium [28].

Oxygen produces lager damage as compared to helium and nitrogen because it is a bit heavier than these two and it may be chemically active and higher annealing temperatures and may can affect the electrical properties of the lattice [28].

Zinc produces the highest damage as compared to all the five species used in this work. It is chemically active at higher temperatures and its diffusivity is low as compared to the other species as it is heavier compared to the rest of ion species used to simulate the required test structure [28].

Silicon is the ion specie of choice as its outer most orbit is partially filled, It will not form any bonds with the target atoms, secondly it is neither very heavy nor very light, experimentation can be done at very high as well as relatively lower energies, keeping this in view silicon was used for further experimentation layer by layer. This impact will become more obvious in next chapter where the experimental results of the electrical characterization of AlGaN/GaN devices reveal the influence of the appropriate choice of ion specie to create desirable damage in the lattice for potential engineering of the devices.

CHAPTER 5

EXPERIMENTS, RESULTS & DISCUSSION-II (MEASUREMENTS AND VALIDITY OF MODEL AND DESIGN)

5.1 Introduction:

The III-V semiconductors are currently employed in the fabrication of optoelectronic devices and integrated circuits (IC) for high frequency operations [40-52].Electrical isolation of III–V semiconductors formed by introduction of a controlled concentration of point defects from light ion irradiation is a well-established technique [42-52]. Besides the efficiency of this method to obtain highly isolated layers, it has the additional advantage of maintaining the planarity of the isolated structures [49-51]. Thermal processing of the crystal tends to remove ion beam induced damage and reduce the degree of compensation, while at the same time producing diffusion of the defect centers [44, 47-49]. Therefore thermal processing due to variable implantation temperature and post-implant annealing cycles is crucial to enable electrical and optical characteristics. With the knowledge gained during the design and modeling of ion-beam-engineered AlGaN/GaN HEMT structure thoroughly investigated in the previous sections, a systematic investigation of the real-time experiments carried out on the conventional AlGaN/GaN test structure (already in use commercially and reported in literature on variety of occasions) is presented below:

5.2 Experimental Condition and Details:

The samples studied (test device structure is intentionally chosen to be of the same design as used commercially to independently evaluate the influence of high energy implantation on AlGaN/GaN layers and subsequent impact on the physical properties important to enable frequency and power related device operations) were commercially grown by Metal Organic Chemical Vapor Deposition (MOCVD) on semi-insulating SiC substrate. The 2 Dimensional Electron Gas (2DEG) GaN channel was prepared with sheet carrier concentrations of n_s= $3.1x10^{13}$ /cm^2 and n_s = $3.1x10^{14}$ /cm^2. The damage implantations were carried out by Helium and Silicon ions irradiation at energy of 3000 KeV and 1000 KeV, respectively to place the peak of the damage distribution well inside the substrate as well as the GaN channel making an interface with the AlGaN barrier. A relatively flat damage distribution is created both in the top-layered GaN cap and AlGaN barrier so that a controlled amount of defects may be created at interfaces and surface for possible exploitation during the high power and high frequency applications. These implants were designed and modeled under the scope of this study and carried out at IBS Inc. USA (collaborating R&D) with exact modeled parameters and dimensions. During implantation, the normal to the wafers was inclined at 15° with respect to the beam to minimize ion channeling. The selection of Helium and Silicon for damage studies for these HEMT test structures was crucial. Although the design studies included a range of ion species such as Zinc, Chlorine, Oxygen, Nitrogen etc. but the actual experiments were limited to one inert and lighter ion specie (Helium) and one commonly used dopant in III-V (Silicon, which is not known to create chemical impurity levels in AlGaN/GaN structures unlike Zinc, Chlorine, Oxygen and Nitrogen etc.) so that in-situ thermal effects caused by relatively high energy implantation due to beam heating and self-annealing of defects may be studied in HEMT test devices,

independently. Isolation implants were performed at different combined doses ranging from $5x10^{13}$ cm^{-2} to $2x10^{15}$ cm^{-2} at room temperature (RT). The doped regions under the contact areas were masked using the metal foil on top of those contacts. The resistivity and Hall measurements were carried out using an Ecopia HMS3000 system, whereas HP 4156 parameter analyzer was used to evaluate the DC characteristics. Some of the measurements, implant schedules and annealing cycles were repeated and double checked at facilities in Berkeley National Laboratory, USA

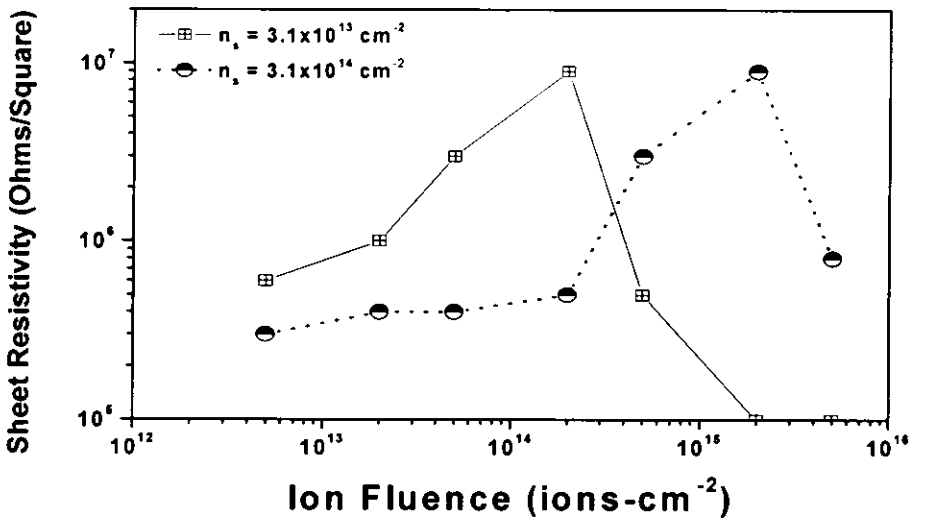

Fig55: Evolution of sheet resistance with the increasing ion dose (experiments designed as similar as depicted in Reference 57 to qualify the model requirements)

5.3 Results and Discussion:

Utilizing the similar model as devised in reference 57, we conducted a very similar experiment to qualify the threshold dose model for III-N-V devices. Following Ref. 50, 52 and 57, a threshold dose for isolation, D_{th}, can be defined as the minimum ion dose at which R_s reaches its maximum value. The presence of

threshold doses can easily be seen in Fig. 5.1, where two distinct threshold doses exist for two different initial sheet carrier concentrations of GaN layers. It has already been demonstrated [50, 52, 57-59] that ion doses required for an effective isolation of GaAs devices have simple linear and reciprocal dependences on the values of initial free carrier concentration and ion-beam-produced atomic displacements, respectively. If n_{so} is the original sheet carrier concentration of the n-type GaN layers, D is the implanted dose to isolate the structure, n_{sD} is the measured sheet carrier concentration after the isolation implantation to dose D then R will be the carrier removal rate which is a function of mass and energy of the ion. The equation relating these parameters is as follows [57]:

$$nso = nsD + RxD\ [57]..... \qquad (5.1)$$

Since we do not intend to fully compensate the layers, optimum carrier removal rate is not considered while designing these experiments. The modelled parameters in terms of accumulated disorder and energy loss due to electronic and nuclear stopping are summarized in Table18 for each case.

Table 19: The modelled physical parameters in response to the high energy ion implantation to the active device regions in nitride HEMT structure are as follows:

PHYSICAL PARAMETERS	3000 KeV He+ into SiC at Rp (10.7 microns)	3000 KeV He+ into GaN Channel (3 microns)	1000 KeV Si+ into GaN Channel at Rp (1.45 microns)
Energy loss due to Electronic Deposition (electron volt/angstrom)	11.98	23	14.88
Energy loss due to Nuclear Deposition (electron volt/angstrom)	0.19	2.46	21
Accumulated Disorder %	7.3	1.9	15.1

The threshold doses in this experiments are $D = 2x10^{14}$ cm^{-2} and $D = 2x10^{15}$ cm^{-2} for the n-type GaN layers with initial channel sheet carrier concentrations of $3.1x10^{13}$/cm^2 and $3.1x10^{14}$/cm^2, respectively. Figures 56 and 57 illustrate the isolation characteristics (resistivity) for different starting material layers implanted with combined implantation at RT for a range of doses including the threshold doses in each case. Each data point is comprised of the cumulative isochronal annealing sequence for 50s period. For the D_{th} case in Fig. 56, the stability of the isolation is restricted to temperatures below 400 °C.

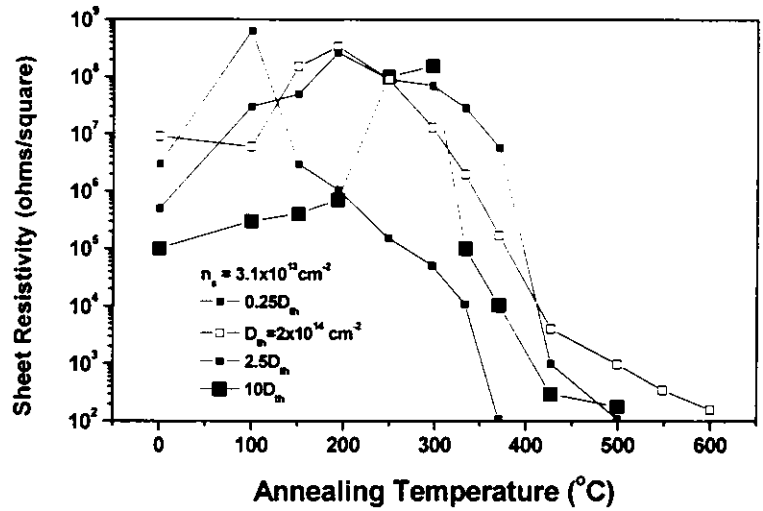

Fig 56: *Carrier Removal characteristics (sheet resistance versus post-implant annealing temperature) for AlGaN/GaN device structures of initial sheet carrier concentration of* $3.1x10^{13}$ *cm*$^{-2}$ *in GaN channel.*

In the samples irradiated to doses higher than the threshold dose ($2.5D_{th}$) the isolation persists up to the temperature of 350 °C. The increase of the irradiation dose to $10D_{th}$ leads to the decrease of R_s because of hopping conduction in the highly damaged region. During post irradiation annealing there is a progressive increase of R_s with increasing temperature up to 300 °C, since the carrier hopping becomes less effective as the damage is repaired. The defects are removed by annealing above this temperature, which would correspond to the annealing of defect clusters or defect complexes, as already seen in cases such as experiments done in reference 57 and references therein.

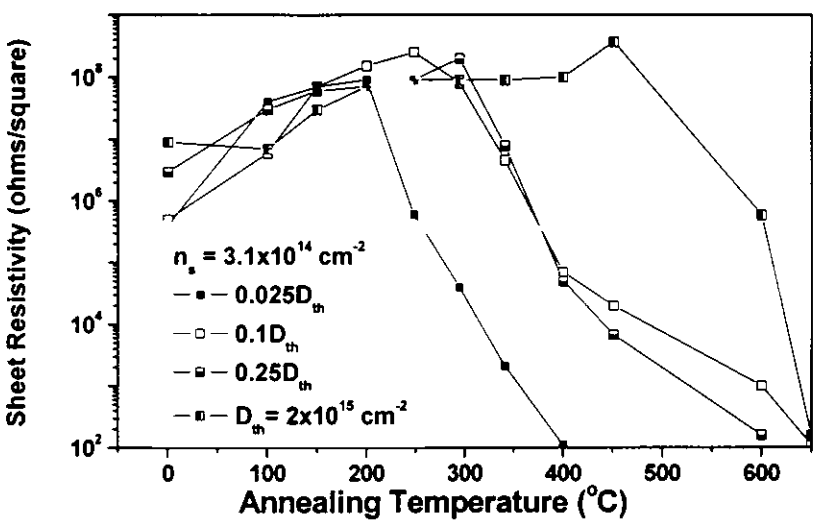

Fig 57: Presence of persistent electrical compensation: thermally stable process window for combined Helium and Silicon Implantation-compensated AlGaN/GaN device structures of initial sheet carrier concentration of $3.1x10^{14}$ cm^{-2} in GaN channel. These structures are implant-isolated at RT for a range of doses including the threshold doses in each case. Each data point is comprised of the cumulative isochronal annealing sequence for 50s period.

Figure 57 also explains that the devices of starting material with high sheet channel carrier concentration are reasonably isolated with threshold doses. Further higher doses, for example in the case of Fig. 56, are not needed to obtain better isolation. The larger thermally stable window (till 500°C) achieved in the case of the results shown in figure 57, is sufficient for subsequent processing such as contact sintering. The evolution of sheet resistivity with varying annealing temperatures at certain ion fluence (variable doses with respect to the already calculated threshold doses in Fig 55) shown in Figure 56 and 57 follow the similar trend and behave almost identically to a similar finding in case of GaAs layers isolated with protons [79]. This is expected as the post-implant-annealed-isolation trends are reported to behave in a similar fashion for most of the III-V devices, particularly for damage-only ion species such as protons, helium and silicon [42-51, 79].

As part of our study, we aimed to employ the technique of ion beam engineering onto the scheme of commercially designed AlGaN/GaN HEMT structures. While using the modelled parameter of Threshold Dose during the ion implantation, it is experimentally shown above that one can make the layers highly resistive and hence the extent of mobile electrons can be reduced according to the requirements of the device operations. One can achieve a fully compensated layer either in capped layer, barrier layer, channel, buffer or substrate. The design and modelling of ion implantation parameters, such as in our experiments, provide us a flexibility to control the amount of mobile carriers within a certain layer or interface, which may in turn be utilized to control the high-power and high-frequency operations. The usage of high energy implantation (particularly the MeV range of incident energies) is known to produce special defect complexes due to the dynamic annealing during the process of implantation. Therefore, such

thermal effects also contribute in the significant results achieved after the implantation in form of physical changes experienced by the lattice. With the scope of high electron mobility transistor's operation in mind, our proposed design of ion implantation parameters also provide an effective solution to improve the efficiency of device characteristics. Being used in RF/Microwave amplification environment, nitride HEMT devices are considered to have efficiencies to operate both in low and high field carrier transport. This demands a high carrier density along with high carrier mobility even during the relatively high temperature environments. Persistent low sheet resistivity and high 2DEG mobility is desirable physical attribute of such devices. This can be only achieved if we fabricate the HEMT structure with (a) high spatially distributed conductivity of GaN channel, and (b) high quality of AlGaN/GaN interface. The higher strain and better carrier confinement on AlGaN/GaN interface may provide a desirable quality lower sheet resistivity as well as higher 2DEG mobility. We suggest that by using the high energy ion implantation with a uniformly distributed damage distribution in the capped layer (near surface regions) and peak of the damage profile within the channel with a reasonable extent of damage therein may create such defects within the lattice which may confine the carriers at the interface effectively. The follow-up annealing at a certain temperature, while recovering the lattice after ion irradiation, may release an additional amount of the trapped carriers in the channel which in turn would raise the mobility of the electron gas. Ion implanted structures may consequently exhibit better output device characteristics by virtue of getting damaged to an extent where they form defects which help the interface relax in such a manner that while undergoing the reversal effect (annealing to recover the ion-induced damage) they provide more carriers to the channel with greater mobility and lower sheet resistivity. This way, relatively higher initial carrier density materials may also be used to perform device operations exactly the same

way as could be done with lower initial carrier densities in AlGaN/GaN structures. Therefore, our suggested ion implantation model and designed experiments provide a substantial control on the carrier transport mechanisms while looking at the output device characteristics of AlGaN/GaN HEMT structures. This discussion is exhibited in Fig.5.4, where initial sheet carrier concentration is plotted against the 2DEG hall mobility in AlGaN/GaN layers for HEMT structures with and without implantation. The samples which were irradiated with combined implantation schedule of Helium and Silicon ions, received the fluence which was at least two orders of magnitude below the threshold doses that were used in earlier experiments for each independent case of initial sheet carrier concentration. This is due to the fact to produce light damage in the lattice which is neither stable nor long range to compensate the layer fully. This is an extent of ion-induced damage which is just about sufficient to trap the carriers at interface and recoverable at a low thermal budget. Figure 4 clearly shows that the higher values of 2DEG mobility are achieved when the HEMT structures have undergone a carefully designed ion implantation and annealing at temperatures around 400^{o}C.

This trend is repeatable for starting materials with different initial carrier densities.

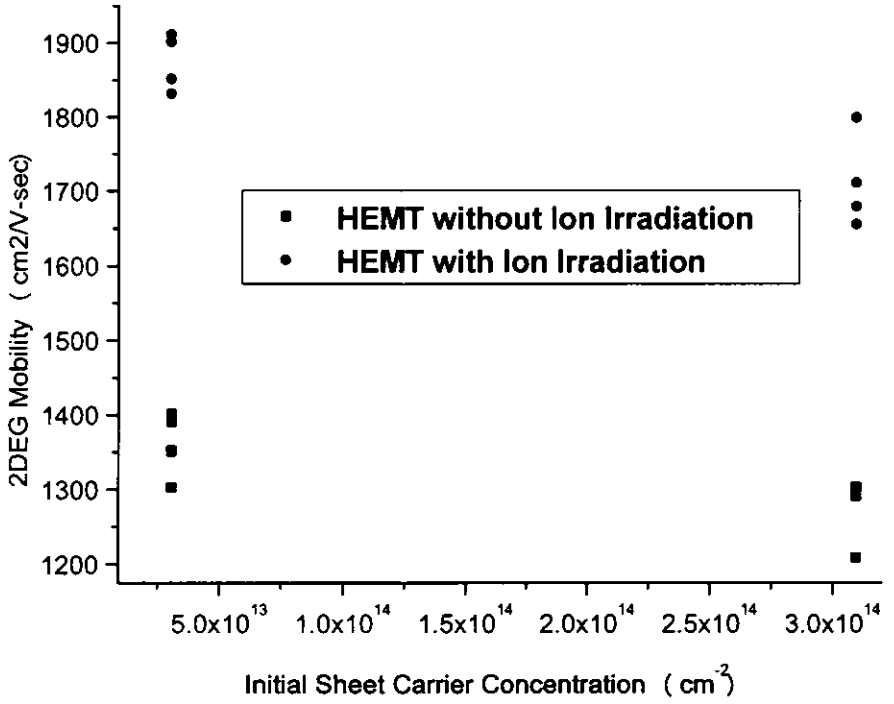

Fig 58: 2DEG Hall mobility versus initial channel carrier density (n_s= 3.1x10^{13} cm^{-2} and n_s= 3.1x10^{14} cm^{-2}) for AlGaN/GaN structures with and without ion implantation and annealing cycles (combined He^+ and Si^+ implants with ion doses 2 orders of magnitude lesser than the Threshold Dose in each case as shown in Fig.5.1)

The data points shown in all the curves presented in Figure 55 to 60 are average of repeated measurements of each hall sample used in this study. A converse is plotted in Figure 59 where sheet resistivity is plotted against the starting carrier density of AlGaN/GaN HEMT structure for cases where the

structures are measured with and without the ion irradiation received.

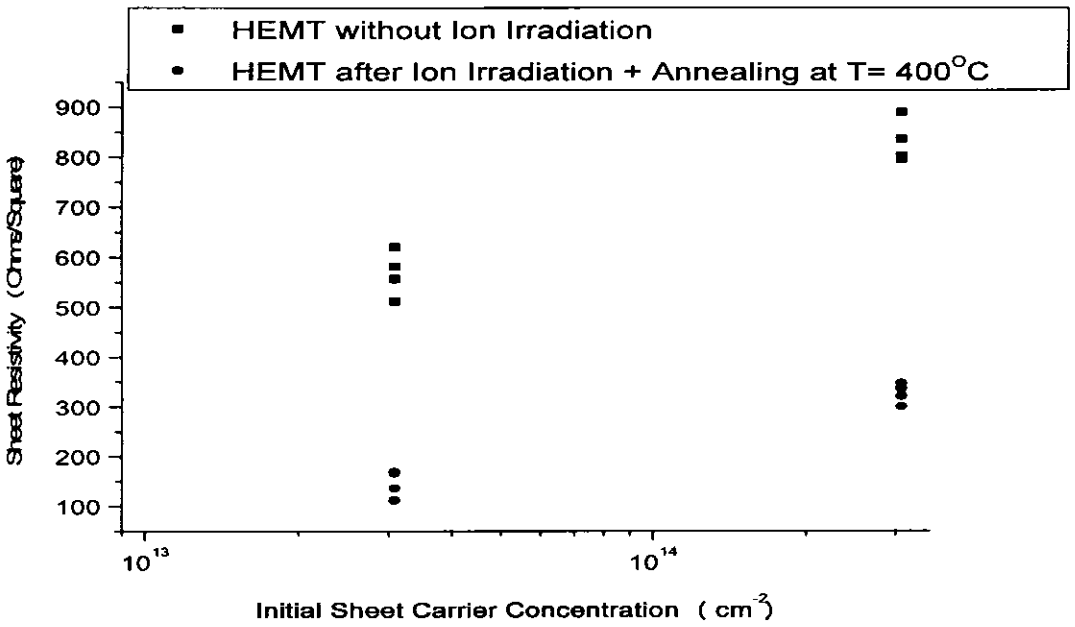

Fig 59: Sheet Resistivity versus initial channel carrier density (n_s= 3.1x10^{13} cm^{-2} and n_s= 3.1x10^{14} cm^{-2}) for AlGaN/GaN structures with and without ion implantation and annealing cycles (combined He^+ and Si^+ implants with ion doses 2 orders of magnitude lesser than the Threshold Dose in each case as shown in Fig. 55)

A converse pattern is achieved as compared to Figure 58. It is interesting to note that the lattice engineering due to the carefully designed ion implantation schedule and subsequent rapid thermal annealing provided a very low value of sheet resistivity (~100 ohms/square) which is better than many commercial devices manufactured by conventional process routines without introducing lattice normalization engineering by ion implantation. Both the lower values of sheet resistivity and higher value of 2DEG mobilities are vital to improve the RF characteristics of the HEMT device for small signal applications. Figure 60 exhibits the characteristic trends of extrinsic transconductance (G_m) and drain

current density (I_{DS}) versus the gate voltage (V_g). The measurements were performed with the V_{DS} = 5 Volts supplied to the structure having gate dimensions of 0.4x220 μm^2. A maximum value transconductance of over 300 mS/mm was achieved for ion-implanted structures, which is better than the average commercial HEMT structure without undergoing the post process ion implantation and annealing cycles. The results presented in Figure 58, 59 and 60 have ramifications for device and design engineers who are particularly looking at the possibilities of optimizing the AlGaN/GaN HEMT efficiency for high-power and high-frequency operations.

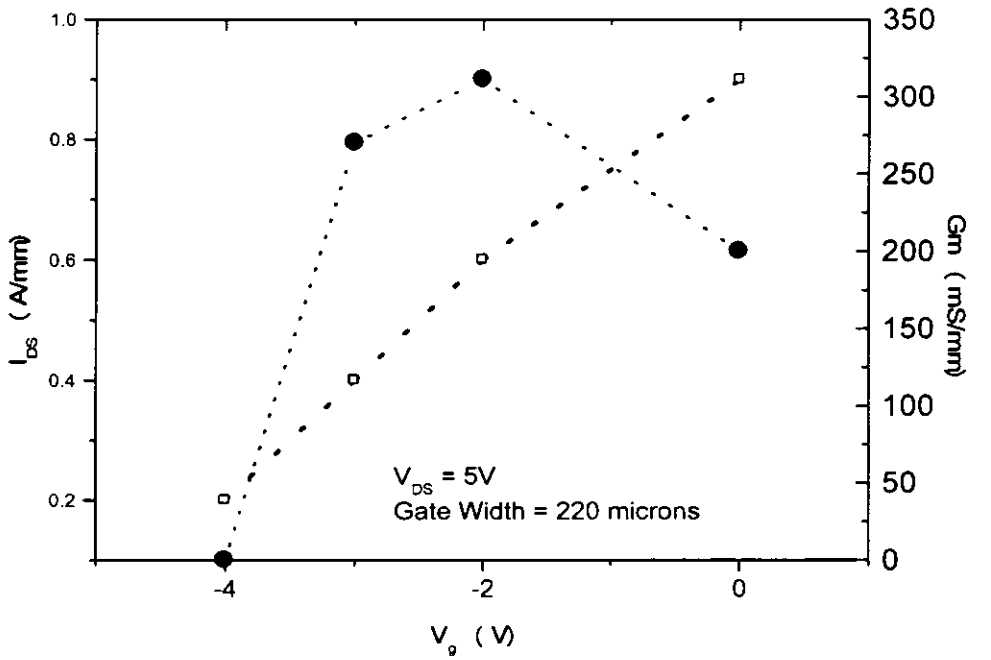

Fig60: Characteristic trends of extrinsic transconductance (G_m) and drain current density (I_{DS}) versus the gate voltage (V_g)

CHAPTER 6
CONCLUSION & FUTURE WORK

6.1 Conclusion

The ion implanted AlGaN/GaN High Electron Mobility Transistors (HEMT) test structures were studied thoroughly to look into the possibilities of enhancing the HEMT efficiency for high-power and high-frequency electronic applications. With the results of this detailed study, we conclude the following:

- A dedicated experimental design was created in order to study the influence of the physical parameters in response to the high energy (by virtue of in-situ beam heating due to highly energetic implantation) ion implantation to the active device regions in nitride HEMT structures. Several sets of simulations were performed to predict the appropriate experimental conditions during the process of ion implantation induced damage formation before the test structure actually undergone the ion irradiation. A very calculated disorder or damage created in the HEMT structure was then studied carefully with Electrical characterization techniques such as Hall, I-V and G-V measurements.

- The evolution of the electrical characteristics affecting the high-power and high-frequency operations was also analyzed by subjecting the HEMT active device regions to the progressive time-temperature annealing cycles.

- The influence of relatively damaged HEMT structure by using "carefully" designed ion irradiation protocols was compared with the ones which are commercially available (having no post-process implantation protocols experimented) and it revealed that by changing the ion-induced physical dynamics of the channel and interface regions in AlGaN/GaN HEMT structures may enhance the operational efficiency of the device in many ways.

- The suggested model can also provide a functional process window to control the extent of 2D Electron mobility in the AlGaN/GaN HEMT devices undergoing a full cycle of thermal impact i-e from a desirable conductive region to a highly compensated one. That is shown possible by engineering the HEMT structures with or without the irradiation of so-called Threshold Doses (D_{th}) and their consequent impact on the carrier density of the channel in the AlGaN/GaN HEMT devices. The evolution of such a physical impact is also studied by varying the annealing temperatures to devise process instruments for various operational domains in AlGaN/GaN HEMT structures. The work carried out in this study is very important for the semiconductor process engineering and have ramifications for device engineers.

6.2 Further Work

A lot of possibilities arise during the course of this study, which may form the basis of detailed further work to address the problem areas more in depth and rigorously. Some of the ideas are discussed as below:

- The influence of hot and cold implantation (implantations carried out at elevated and below room temperature) on HEMT devices may be studied to control the dynamics of 2D electron motilities, which in turn would play a major controlling role in high-frequency and high-power device operations;

- The thermal and temporal stability of the effects maintained by the carefully designed ion irradiation parameters may be of interest to monitor the device's operational behavior in extreme conditions (such as extreme pressure and extreme temperatures etc.);

- The structural changes occurred to the interfaces and channel areas after the ion implantation and during the time-temperature annealing cycles may impact the structural dynamics necessary to provide a minimum number of free carriers in the channel region to effectively perform the high-frequency operations. A physical study (using the techniques such as Rutherford Backscattering Spectroscopy, Field-Emission Scanning Electron Microscopy etc.) may be carried out on the samples used in our study to correlate the structural dynamics with the efficiency and stability of the electrical characteristics exhibited on as-implanted and post-processed AlGaN/GaN HEMT devices.

References:

[1]. Stopping and Range of Ions in Matter (SRIM) by James F.Ziegler, SRIM.Org.Annapolis MD 21402, USA.2010

[2]. http;/www.fqd.fujitsu.com/Hemt/(Spring 2002)(web reference)

[3]. http;//www.fqd.fujitsu.com/Hemt/(Spring 2002)(web reference)

[4]. William J.Roman, Development of AlGaN/GaN HEMT Technology for Highest Frequency Operation,2008.

[5]. Stephen a. Campbell, The Science of Engineering of microelectronics technology 2nd edition, Oxford University Press,2001

[6]. Vittoria Privitera. Ultra low energy ion implantation of Boron for Future silicon devices. Current Opinion in Solid State and Material Sciences, Volume 6, Issue 1, Page 55-65, February 2002.

[7]. Rajan V. nagabushnam, Rajiv K. Singh and Sujit Sharan, Dopant diffusion Studies and free carrier lifetime during rapid thermal processing of semi conductors. Materials Science in Semiconductor Processing, Volume 1, Issue 3-4, Pages 207-218, December, 1998.

[8]. E. Gilli, V.D. Kunz, C.H, de Groot, T. Uchino, P. Ashburn, D.C. Donaghy, S, Hall, Y. Wang and P.L.F. Hemment Single. Double and surround gate vertical MOSFETs with reduced parasitic capacitance. Solid-State Electronics, Volume 48, Issue 4, Paes 511-519, April 2004.

[9]. Al-Bayati, A. Groui, H. Spear, J. Ito, H. Matsunaga, Y. Ohuchi, K. Miyashita, K. Nakayama, T. Oowada, M. Toyoshima, Y. Advanced CMOS device sensitivity to USJ processes and required accuracy of doing of activation Ion Implantation Technology. 2002. Processing of the 14th International Conference on 22-27 Sept. 2002, pages 185-188.

[10]. Murrell, A.A. Graoui, H. Spear, J. Ito, H. Matsunaga, Y. Ohuchi, K. Al-Bayat, Adachi, K. Miyashita. K. Nakayama. T. Oowada, M. Toyoshima, Y. Doping accuracy requirements of USJ processes for advanced sub-100nm CMOS devices Junction Technology, 2002. IWJT. Extended Abstracts of the Third International Workshop on 2-3 December, 202, pages 9-13.

[11]. B. Colombeau, F. Cristiano, F. Olivie, C. Amanmd, G. Ben Assayag and A. Claverie. Effect of the Ge preamorphization does on boron Diffusion and defect evolution in silicon Nuclear Instruments and Methods in Physics, Research Section B, beam Interactions with Materials and atoms, Volume 186, Issues 1-4, pages 276-280, January 2002.

[12]. J.J. Hamilton, E.J.H. Collart, B. Colombeau, C. Jeynes, M. Bersani, D. Giubertoni, J.A. Sharp, N.E.B. Cowern and K.J. Kirkby. Electrical activation of solid-phase epitaxially regrown ultra-low energy boron implants in Ge preamophization silicon and SOI. Nuclear Instruments and Methods in Physics Research Section B, Beam interactions with materials and atoms, Volume 2237, Issues 1-2, Pages 107-112, August 2005.

[13]. T. Clarysse, D. Vanhaeren, I. Hoflijk and W. Vandervorst. Characterization of electrically active dopant profiles with spreading resistance probe. Materials Science and Engineering, R Reports, Volume 47, Issues 5-6, Pages 123-206, December, 2004.

[14]. Zhong Lin Wang, Yi Liu, Ze Zhang. Handbook of Nanophase and Nanostrcuctured Materials 2003.

[15]. Dr. Talal Alzanki, Antimony Implants for ulta shallow junctions in silicon. Ph. D. Thesis University of Surrey, UK. 2004.

[16]. H. Y. Chan, M.P. Srinivasan, F. Benistant, H.M. Jin and L. Chan Sampling. Calibration of ion implantation profile in crystalline silicon from 0.1 to 300 KeV using Monte Carlo simulation. Solid-State Electronics, Volume 49 issues 7, pages 121-1247, July 2005.

[17]. John O. Borland. Alternative USJ formation and characterization methods for 45 nm node technology. Nuclear Instruments and methods in physics research, Section B, Beam interactions with materials and atoms, volume 237, Issues 1-2, Pages 6-11, August 2005.

[18]. Dieter K. Schroder, semiconductor material and device characterization, 3rd edition 2006, John Wiley & Sons.

[19]. Sorab K. Ghandhi. VLSI fabrication Principles, Silicon and Gallium Arsenide (second edition) 2003 John Wiley & sons (Asia) Ltd.

[20]. F. Lallement and D. Lenoble. Investigation on Boron transient enhanced diffusion induced by the advanced p+/N ultra-shallow junction fabrication processes. Nuclear instruments and methods in physics research, Section B, Beam interactions and materials and atoms, volume 237, Issues 1-2, , Pages 113-120, August 2005.

[21]. O.V. Bushkova, V.M. Zhukovsky, B.I. Lirova and A.K. Kruglyashov fast ion transport in solid polymer electrolytes based on acrylonitrile copolymers solid state ionics, Volume 119, Issues 1-4, Pages 217-222, April 1999.

[22]. Susan K. Earles. Nonmelt Laser annealing of Boron implant silicon. Ph.D. Thesis, University of Florida, 2002.

[23]. Ying Diana Yu. Real-Time Computer Control for Wafer in Rapid Thermal Processing. MS thesis Calgary, Alberta 1997.

[24]. A.T. Fiory. Methods in microelectronics for rapid thermal annealing of implanted Dopants. 11th workshop on crystalline silicon solar cell

materials and process, Edited by B.Sopori, NREL/BK-520-30838, August, 2001.

[25]. P.S. Zory, Quantum Well Laser, Academic Press, 1993.

[26]. G. Wang. S. Tain, M. Morris, S. Morris, B. Obradovic, G. Balamurugan, and A. Tasch, "A computationally efficient ion implant model: Modified Kinchin-Pease Model, "Microelectronic Device Technology, Proceedings of SPIE, (Austin, TX), 1997.

[27]. Asif Bashir Alamni. MS Thesis, Optimizing the process designs of Quantum Well Intermixing for Complex Photonic Integrated Circuits, Department of Physics, COMSATS IIT,August, 2007.

[28]. Stopping and Range of ions in Matter (SRIM) by M.D. Ziegler, James F. Ziegler, SRIM.org. Annapolis, MD 21402, USA,2010.

[29]. Mishra et al, "AlGaN/GaN HEMTs-An Overview of Device Operation and Applications, "Proceedings of the IEEE, Vol.90 PP. 1022-1031, June 2002.

[30]. Jin- YU Shiu, Jui-Chien Huang,\ Vincent Desmaris, chia Ta Chang, Chung-Yu Lu, Kazuhide Kamakura, Toshika Makimoto, Herbert Zirath, Member IEEE Niklas Rorsman, and Edward Yi Chang, Senior member IEEE, Oxygen Ion Implantation Isolation Planar Process for AlGaN/GaN HEMT's, IEEE Electron Device Letters, Vol. 28 No.6 June 2007.

[31]. J S Wang, S H Yu, Y R Lin, C S Yang, T T Chen, Y F Chen, G W Shu, J L Shen, R S Hsiao, J F Chen and J Y Chi. Optical and structural properties of vertically stacked and electronically coupled quantum dots in InAs/GaAs multilayer structures. Nanotechnology 18, 015401, 2007

[32]. P. Lever, L. Fu, C. Jagadish, M. Gall and HH. Tan. Interdiffusion in Semiconductor Quantum Dot Structures. Mat. Res. Soc. Symp. Proc. Vol 744 2003 Materials Research Society,2003

[33]. H.H Tan, L. Fu, M.B. Johnson, L.V. Dao, M. Gal and C. Jagadish. Improved intermixing in GaAs/AlGaAs quantum well structures through repeated implantation anneal sequence. Department of Electronic Materials Engineering Research School of physical Sciences and Engineering The Australian National University Canberra, Australia,1998.

[34]. Ion Implantation of Si, Mg and C into A10.2G-88N. Solid-state Electronics Vol.41, No.5, pp. 703-706 1997.

[35]. Anirban Basu, A-Vipran Kumar, and Ilesanmi Adesida. Study of Fluorine bombardment on the electronic properties of AlGaN/GaN hetrostructures. Micro and Nanotechnology Laboratory and Department of Electrical and computer Engineering, University of Illinois at Urbana-Champaign, Urbana, Illinois 61801,2007.

[36]. Hongwei Chen, Maojun Wang, Kevin J. Chen. Enhancement mode AlGaN/GaN HEMTs fabricated by standard Fluorine Ion Implantation. Dept of Electronic and Computer Engineering, Hong Kong University of Science and Technology, Hong Kong,2010.

[37]. M. B Johnston, M. Gal, Na Li, Zhanghai Chen, Xingquan Liu, Ning Li, Wei Lu, and S. C. Shen, L. Fu, H. H. Tan, and C. Jagadish. Interdiffused quantum-well infrared photodetectors for color sensitive arrays. Volume 75, Number 7, Applied Physics Letters, 16 August 1999

[38]. Erik J. Skogen, Larry A. Coldren, James W. Raring and Steven P. DenBaars. Multiple-band-edge quantum-well intermixing in the

InGaAs/InGaAsP/InGaP material system. Applied Physics Letters 86, 241117, 2005.

[39]. Na Li, Ning Li, W. Lu, X. Q. Liu, X. Z. Yuan, Z. F. Li, H. F. Dou and S. C. Shen. Proton implantation and rapid thermal annealing effects on GaAs/ AlGaAs quantum well infrared photodetectors. Superlattices and Microstructures, Vol 26, Page#317-24,1999.

[40]. N. V. Kryzhanovskaya, A. Y. Egorov, V. V. Mamutin, N. K. Polyakov, A. F. Tsatsulinikov, Y. G. Musikhin, A. R. Kovsh, N. N. Ledentsov, V. M. Ustinov, and D. Bimberg, Semicond. Sci. Technol. **20**, 961,2005.

[41]. S. R. Kurtz, N. A. Modine, E. D. Jones, A. A. Allerman, and J. F. Klem, Semicond. Sci. Technol. **17**, 843,2002.

[42]. S. Ahmed, P. Too, R. Gwilliam, and B. J. Sealy, Appl. Phys. Lett. **79**, 3533,2001.

[43]. S. Ahmed, K. Amirov, U. Larsson, J. Lin, A. Haq, P. Too, and Z. Tabatabaian, Vacuum, **78**, 137,2005.

[44]. S. Ahmed, J. Lin, A. Haq, and B. Sealy, Nucl. Instrum. Meth. Phys. B. **240**, 214,2005.

[45]. S. Ahmed, J. Lin, A. Haq, B. Sealy and R. Gwilliam. Nucl. Instrm. Meth. Phys. B **237**, 102,2005.

[46]. S. Ahmed, R. Gwilliam, and B. J. Sealy, Semicond. Sci. Technol. **16**, 28,2001.

[47]. S. Ahmed, A. P. Knights, R. Gwilliam and B. J. Sealy, Semicond. Sci. Technol. **16**, 17,2001.

[48]. S. Ahmed, R. Gwilliam, and B. J. Sealy, Semicond. Sci. Technol. **16**, 64,2001.

[49]. S. Ahmed, R. Nawaz, R. Taiq, K. Amirov, U. Larsson and W. A. Syed. Appl. Phys. Lett. **91**, 062112,2007.

[50]. H. Boudinov, A. V. Coelho, and J. P. DeSouza, J. Appl. Phys. **91**, 6585, 2002.

[51]. S. J. Pearton, Mater. Sci. Rep. **4**, 313,1990.

[52]. I. Danilov, J. P. DeSouza, and H. Boudinov, J. Appl. Phys. **92**, 4261, 2002.

[53]. J. F. Ziegler, J. P. Biersack, and U. Littmark, *The Stopping and Range of Ions in Solids* Pergamon, Oxford, 1985.

[54]. R. G. Hunsperger, *Integrated Optics: Theory and Technology* Springer, Berlin, 1982.

[55]. T. S. Moss. *Optical properties of Semiconductors* Butterworths, London, 1959.

[56]. S. Somekh, E. Garmire, A. Yariv, H. L. Garvin, R. G. Hunsperger, Appl. Opt. **13**, 327,1974.

[57]. S. Ahmed, B. J. Sealy, and R. Gwilliam. *IEEE Technical Digest: Electron Devices for Microwave and Optoelectronic Applications*, 18,2002.

[58]. J. P. deSouza, I. Danilov, and H. Boudinov, J. Appl. Phys. **81**, 650,1997.

[59]. J. P. de Souza, I. Danilov, and H. Boudinov, Appl. Phys. Lett. **68**, 535,1996

[60]. http://www.nist.gov/pml/div683/hall_resistivity.cfm (web reference)

[61]. A.Chvala, D. Donoval, R. Sramaty, J. Marek, J. Kovac, P. Kordos, and J. Skrinarova. Characterization of electrical properties of AlGaN/GaN Schottky diode at very high temperature. Department of microelectronics, Slovak University in Bratislava 3 Ilkovikova 3, 812, 19 Bratislava, Slovakia.

[62]. Zhiyong Ma, Xiaoliang Wang, Guoxin Hu, Junxue Ran, Xinhua Wang, Baozhu Wang, Baozhu Wang, Weijun Luo, Jianpin Li. MOCVD grown AlGaN/AIN/GaN HEMT structure with compositionally step-graded AlGaN barrier layer. Institute of semiconductors, Chinese academy of science Beijing 100083 China,2006.

[63]. Jin-Yu Shiu, Jui-Chien Huang, Vincent Desmaris, Chia-Ta Chang, Chung-Yu Lu, Kazuhide Kumakura, Toshiki Makimoto, Herbert Zirath, Member IEEE, Niklas Rorsman, and Edward Yi Chang, Senior Member, IEEE. IEEE ELECTRON DEVICE LETTERS, VOL.28 NO.6 2007.

[64]. E.L. Piner, D.M. Keogh, J.s. Flunn, and J.M. Redwing. AlGaN/GaN High Electron Mobility Transistor Structure Design and Effects on Electrical Properties. Spintronics/ATMI, 21002 North 19th Avenue, Suite 5, Phoenix, AZ 85027 ATMI ventures / ATMI, 7 Commerce Drive, Danbury, CT 06810.

[65]. A.Y Polyakov, M Shin, M Skowronski, R.G Wilson, D.W Greve, S.J Pearton, Ion Implantation of Si, Mg and C in to AlO.2Ga 0.88N, Solid-State Electronics, Volume 41, Issue 5, pp. 703-706, 1997

[66]. Anirban Basu, a- Vipan Kumar, and Ilesanmi Adesida. Study of fluorine bombardment on the electronic properties of AlGaN/GaN heterostructures. Micro and Nanotechnology Laboratory and Department of Electrical and Computer Engineering, University of Illinois at Urbana- Champaign, Urbana, Illinois 61801,2007.

[67]. Undoped AlGaN / GaN HEMTs for Microwave Power Amplification. IEEE TRANSACTIONS ON ELECTRON DEVICES, VOL. 48, NO.3, 2001.

[68]. High-Power Microwave GaN/AlGaN HEMT's on Semi-Insulting Silicon Carbide Substrates. IEEE ELECTRON DEVICE LETTERS, VOL. 20, NOV. 4, 1999.

[69]. Hongwei Chen, Maojun Wang, Kevin J. Chen. Enhancement-mode AlGaN/GaN HEMTs fabricated by standard Fluorine Ion Implantation. Dept. of Electronic and Computer Engineering, Hong Kong University of Science and Technology, Hong Kong,2010.

[70]. Ahmed Shuja. Ion Beam Application to Next Generation Microelectronics: Micro and Nanoelectronics: Photonics, Daya Publishing House.Dehli,India,50-58,2009.

[71]. Qian Feng, Li-Mei Li, Yue Hao,Jin-Yu Ni, Jin-Cheng Zhang. The improvement of ohmic contact of Ti/Al/Ni/Au to AlGaN/GaN HEMT by multi-step annealing method. The institute of Microelectronics, Xi' Dian University, Xi' 710071, China June 2009.

[72]. Jaesun Lee, Dongmin Liu, Hyeongnam Kim, Wu Lu .Post annealing effects on device performance of AlGaN/GaN HEMT. Department of Electrical Engineering, The Ohio State University, 205 Dreese Labs, 2015 Neil Avenue, Columbus, 2004.

[73]. S. Jha a, Emil V. Jelenkovic´ b, M.M. Pejovic´ c, G.S. Ristic´ c, M. Pejovic´ c, K.Y. Tong b, C. Surya b, I. Bello a,W.J. Zhang.,Stability of submicron AlGaN/GaN HEMT devices irradiated by gamma rays, Microelectronic Engineering volume 86, issue 1, pp37-40, 2009

[74]. Eungsun Byon, Jong-Kuk Kim, Jong-Joo Rha, Sik-Chol Kwon, Zongxin Mu, Cui Liu, Guoqing Li. Effects of metal ion implantation on thermal instability of diamond-like carbon films., Surface and Coating technology, volume 201, issue 15, pp 6670-6673, 2007.

[75]. Mukesh Kumar, Rajkumar, P.M. Raole, S.K. Gupta, Dinesh Kumar, P.J. George. Effect of Plasma immersion ion implantation on the thermal stability of diffusion barrier layers. Surface & coating technology,186,pp 77-81,2004.

[76]. J. A. Romano, E.C da Silva, L. F. Schelp, J.E. Schmidt, R. Meckenstock, J. Pelzl. Effects of Ar-ion implantation and thermal treatment on magnetic properties of Co/Pd multilayer: a ferromagnetic resonance study,pp#161-169,1999.

[77]. Adam Perlinger, Seenivasan Subramanium, Vinesh Sukumar, Harry W. Li, Herbert L. Hess. Temperature-Independent High Voltage Reference Design in Silicon-Insulator CMOS Technology,Vol.3,pp#3231-3234,2004

[78]. Umesh K. Mishra, S. Brown, M.J Delaney, Paul T. Greiling, and Charles F. Krumm, .The AlInAs-GaInAs HEMT for Microwave and Millimeter-Wave Applications, vol 37,pp# 1279-1285,1989.

[79]. S. Ahmed, K. Amirov, U. Larsson, P. Too, B. J. Sealy and R. Gwilliam, Thermal processing effects in proton-isolated n-type GaAs devices, IEEE Technical Digest: Electron Devices for Microwave and Optoelectronic Applications, Pg 210-216, 2003.